Journal of the Mechanics and Physics of Solids 119 (2018) 298–318

Contents lists available at ScienceDirect

Journal of the Mechanics and Physics of Solids

journal homepage: www.elsevier.com/locate/jmps

Wrinkles in soft dielectric plates

Yipin Su[a,b], Hannah Conroy Broderick[a], Weiqiu Chen[b], Michel Destrade[a,b,*]

[a] School of Mathematics, Statistics and Applied Mathematics, NUI Galway, University Road, Galway, Ireland
[b] Department of Engineering Mechanics, Zhejiang University, Hangzhou 310027, PR China

ARTICLE INFO

Article history:
Received 31 March 2018
Revised 29 June 2018
Accepted 1 July 2018
Available online 4 July 2018

Keywords:
Dielectric plates
Large actuation
Snap-through
Wrinkling instability

ABSTRACT

We show that a smooth giant voltage actuation of soft dielectric plates is not easily obtained in practice. In principle one can exploit, through pre-deformation, the snap-through behavior of their loading curve to deliver a large stretch prior to electric breakdown. However, we demonstrate here that even in this favorable scenario, the soft dielectric is likely to first encounter the plate wrinkling phenomenon, as modeled by the onset of small-amplitude sinusoidal perturbations on its faces. We provide an explicit treatment of this incremental boundary value problem. We also derive closed-form expressions for the two limit cases of very thin membranes (with vanishing thickness) and of thick plates (with thickness comparable to or greater than the wavelength of the perturbation). We treat explicitly examples of ideal dielectric free energy functions (where the mechanical part is of the neo-Hookean, Mooney–Rivlin or Gent form) and of dielectrics exhibiting polarization saturation. In addition to the expected buckling mode coming from the purely elastic case, we discover a second mode occurring at large voltages in extension. We find that plates always wrinkle anti-symmetrically, before the symmetric modes can be reached. Finally, we make the link with the classical results of the Hessian electro-mechanical instability criterion and of Euler buckling for an elastic column.

1. Introduction

When a soft dielectric plate is put under a large voltage applied to its faces, it expands in its plane. At first, the expansion increases slowly and almost linearly with the voltage until, typically, a local maximum is reached. Then in theory, the voltage drops suddenly, until it reaches a local minimum, rises again, to reach the same level it had at the earlier maximum, and then continues to rise. In practice the voltage does not drop: it stays at the level of the first maximum while the plate expands rapidly, until it starts increasing again with the stretch. The membrane is said to experience a *snap-through expansion* (An et al., 2015; Dorfmann and Ogden, 2014b; Li et al., 2017; Rudykh and Bhattacharya, 2012; Zhao and Suo, 2010). This large and almost instantaneous extension is highly desirable in experiments but is rarely achieved because during the snap-through the elastomer fails due to *electric breakdown* (Blok and LeGrand, 1969; Huang et al., 2012b; Koh et al., 2011). Graphically, the curve of the electric breakdown crosses the voltage-stretch curve before the snap-through portion is completed.

This undesirable outcome can be avoided in a number of ways, in principle (Jiang et al., 2015; 2016; Koh et al., 2011; Li et al., 2011a). We could for instance try to design a dielectric material with a free energy density such that the snap-through

* Corresponding author at: School of Mathematics, Statistics and Applied Mathematics, NUI Galway, University Road, Galway, Ireland.
E-mail address: michel.destrade@nuigalway.ie (M. Destrade).

https://doi.org/10.1016/j.jmps.2018.07.001
0022-5096/

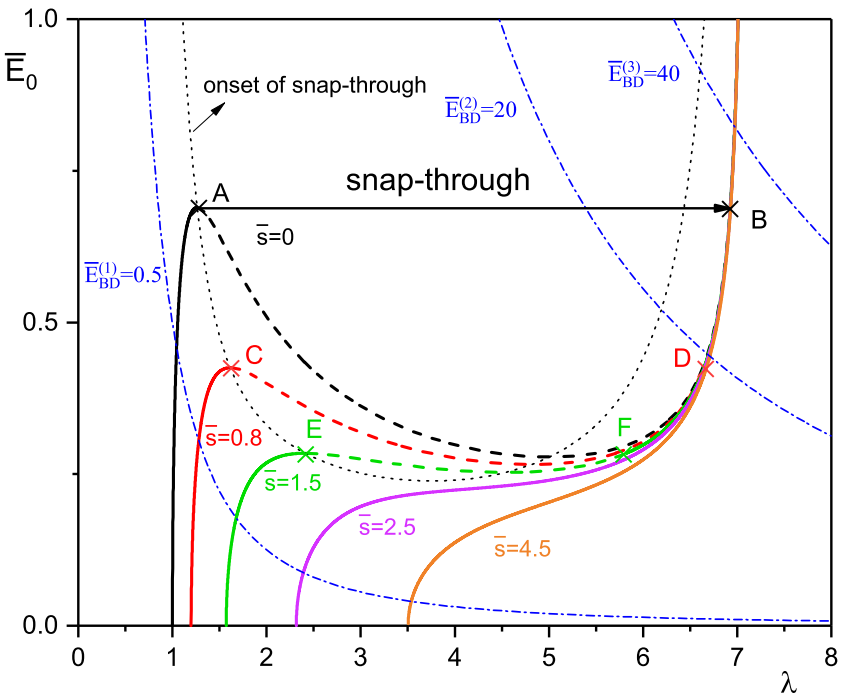

Fig. 1. Principle of the snap-through giant actuation. Solid lines are the voltage-stretch curves for homogeneous loading at different levels of pre-stress ($\bar{s} = 0, 0.8, \ldots, 4.5$), when the plate is modeled by the Gent ideal dielectric (here $J_m = 97.2$ Dorfmann and Ogden, 2014b; Gent, 1996). Dotted line corresponds to the onset of snap-through instability. The dashed parts of the voltage-stretch curves are the theoretical response of the elastomer after the snap-through instability is triggered, which will not happen in practice. The blue dashed–dotted lines are hypothetical Electrical Breakdown curves. The situation described by $\overline{E}_{BD}^{(3)}$ is the most favorable, allowing the initially unstretched material to expand and experience a large snap-through from A to B. For $\overline{E}_{BD}^{(2)}$, this will not be allowed, but a certain level of pre-stress (here $\bar{s} = 0.8, 1.5$) will give a (smaller) snap-through transition (from C to D, from E to F, respectively). As the hypothetical $\overline{E}_{BD}$ curve slides down further, this possibility will vanish eventually (see $\bar{s} = 2.5, 4.5$ curves). For $\overline{E}_{BD}^{(1)}$, no snap-through is possible. (For interpretation of the references to color in this figure legend, the reader is referred to the web version of this article.)

sequence is completed prior to electrical breakdown. But it seems that such a material has not been synthesised yet. We could pre-stretch the membrane so that the snap-through path is shifted below that of the un-stretched membrane. But in that scenario the snap-through actuation gain is greatly reduced. Moreover, with larger pre-stretch, the corresponding path might become increasing monotonic and the snap-through possibility will then disappear altogether.

These possible events are summarised in Fig. 1, where we take a Gent ideal dielectric with $J_m = 97.2$ (Dorfmann and Ogden, 2014b; Gent, 1996) as a representative stiffening parameter of elastomers (a different value stretches or shrinks the plots, but the essential results remain the same). The critical dimensionless electric field of the plate is $\overline{E}_{BD} = V_{BD}/(h\sqrt{\mu/\varepsilon})$, where V_{BD} is the voltage causing electrical breakdown of the elastomer and h is its current thickness. This material constant $\overline{E}_{BD}$ is also known as the *dielectric strength* (Pelrine et al., 2000). For an equal-biaxially stretched dielectric elastomer, $\overline{E}_{0BD} = \lambda^{-2}\overline{E}_{BD}$, where $\overline{E}_{0BD}$ is the nominal measure of $\overline{E}_{BD}$ and λ is the in-plane stretch. This relation is displayed by the blue dashed–dotted lines in Fig. 1, for hypothetical values of the dielectric strength ($\overline{E}_{BD} = 0.5, 20, 40$).

In this paper we show that in any case, the snap-through scenario is derailed because the loading curve crosses that of *wrinkle formation*. Indeed, several experiments (Jiang et al., 2015; 2016; Liu et al., 2016; Plante and Dubowsky, 2006) have shown that sinusoidal wrinkles appear in soft dielectric plates under high voltage, see examples in Fig. 2. Here, we model and predict how they will form.

In Section 2, we begin by recalling the equations governing the large deformation of a dielectric plate subject to pre-stretch and voltage.

We then rely on the theory of incremental deformations superposed on large actuation (Bertoldi and Gei, 2011; Bortot and Shmuel, 2018; Dorfmann and Ogden, 2010a; 2010b; Gei et al., 2012; Rudykh et al., 2014; Rudykh and deBotton, 2011; Su et al., 2016) to solve the boundary value problem of small-amplitude sinusoidal wrinkles appearing on the mechanically-free faces of the plate (Section 3).

This problem was treated earlier by Dorfmann and Ogden (2014a,c) and more recently, by Yang et al. (2017b) and Díaz-Calleja et al. (2017), but not in a fully analytical manner as here. Here, we present a general framework to solve the boundary-value problem for a general free energy density. We manage to obtain analytical results in the case of the Gent ideal dielectric, a model which exhibits the typical non-monotonic snap-through loading curve, see Fig. 1, and also in the cases of neo-Hookean and Mooney–Rivlin ideal dielectrics. Thanks to the Stroh formulation and the surface impedance

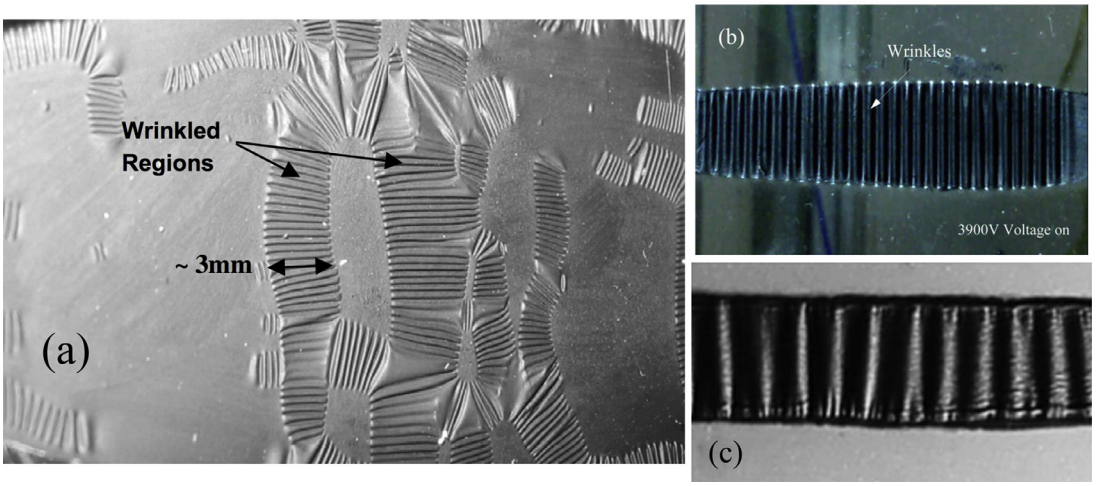

Fig. 2. Experimental evidence of electro-mechanical wrinkling instability: (a) collapse of a thin film of the rubber-like material VHB 4905/4910 put under a large voltage (Plante and Dubowsky, 2006); (b) wrinkling of a VHB 4910 membrane under high voltage (Liu et al., 2016); (c) electric activation of acrylic elastomers (Pelrine et al., 2000). We estimate that the ratio of the initial plate thickness to the wrinkle wavelength is $H/\mathcal{L} \simeq 0.17, 0.35$ in Cases (a) and (b), respectively.

method (Destrade, 2015), we obtain closed-form expressions for the dispersion equation. We are also able to separate the symmetric and antisymmetric modes of buckling and to solve the dispersion equations in a numerically robust manner.

Then in Section 4 we derive the explicit equations giving the thin-plate and the short-wave limits. Plotting the two corresponding curves gives a narrow region where all physical plate dimensions and wrinkle wavelengths are located. We find that it crosses all loading curves before the snap-through can be completed.

In Section 5, we present further results, for dielectric exhibiting polarization saturation, and for the specialization of our analytical formulas to known results in classical Euler buckling theory for elastic columns. We also make the link with, and extend the Hessian criterion of instability (Zhao and Suo, 2007) for electro-elastic dielectrics of a certain thickness.

Finally, Section 6 recapitulates the results and puts them into a wider context, thanks to the extension of the analysis to a tri-axial pre-stretch conducted in the Appendix A.

2. Large actuation

We write the free energy density for the dielectric plate as $\Omega = \Omega(\boldsymbol{F}, \boldsymbol{E}_L)$, where $\boldsymbol{F}$ is the deformation gradient and $\boldsymbol{E}_L$ is the Lagrangian form of the electric field $\boldsymbol{E}$: $\boldsymbol{E}_L = \boldsymbol{F}^T\boldsymbol{E}$. We introduce the following complete set of invariants for an isotropic incompressible dielectric (Dorfmann and Ogden, 2005; 2006; Goshkoderia and Rudykh, 2017; Rudykh et al., 2014),

$$I_1 = \mathrm{tr}\boldsymbol{c}, \quad I_2 = \mathrm{tr}(\boldsymbol{c}^{-1}), \quad I_4 = \boldsymbol{E}_L \cdot \boldsymbol{E}_L, \quad I_5 = \boldsymbol{E}_L \cdot \boldsymbol{c}^{-1}\boldsymbol{E}_L, \quad I_6 = \boldsymbol{E}_L \cdot \boldsymbol{c}^{-2}\boldsymbol{E}_L, \tag{1}$$

where $\boldsymbol{c} = \boldsymbol{F}^T\boldsymbol{F}$ is the right Cauchy–Green deformation tensor.

In the appendix we present results for general materials, where in all generality Ω can be written as $\Omega = \Omega(I_1, I_2, I_4, I_5, I_6)$. In the main text we specialize the results to the *Gent ideal dielectric* (Gent, 1996; Huang et al., 2012a), which exhibits the snap-through response. Its free energy is

$$\Omega_G = -\frac{\mu J_m}{2}\ln\left(1 - \frac{I_1 - 3}{J_m}\right) - \frac{\varepsilon}{2}I_5, \tag{2}$$

where μ is the initial shear modulus in the absence of electric field (in Pa), J_m is the stiffening parameter (dimensionless) and ε is the permitivity (in F/m). When $J_m \to \infty$, the *neo-Hookean ideal dielectric* (Zhao and Suo, 2007) is recovered,

$$\Omega_{\mathrm{nH}} = \frac{\mu}{2}(I_1 - 3) - \frac{\varepsilon}{2}I_5, \tag{3}$$

but that model does not provide snap-through loading behavior.

We call H the initial thickness of the plate. We apply a voltage V on the faces of the plate. Then the only non-zero component of the Lagrangian electric field is $E_{L2} = V/H$, which we call E_0. We call x_1, x_3 the in-plane Eulerian principal axes and x_2 the transverse axis, so that we have the following principal stretches and electric field components,

$$\lambda_1 = \lambda_3 = \lambda, \quad \lambda_2 = \lambda^{-2}, \qquad E_1 = E_3 = 0, \quad E_2 = \lambda^2 E_0. \tag{4}$$

Note that in the appendix we give results for a bi-axially stretched plate, when λ_1 is not necessarily equal to λ_3.

Introducing the function $\omega = \omega(\lambda, E_0)$ as

$$\omega = \Omega(2\lambda^2 + \lambda^{-4}, 2\lambda^{-2} + \lambda^4, E_0^2, \lambda^4 E_0^2, \lambda^8 E_0^2), \tag{5}$$

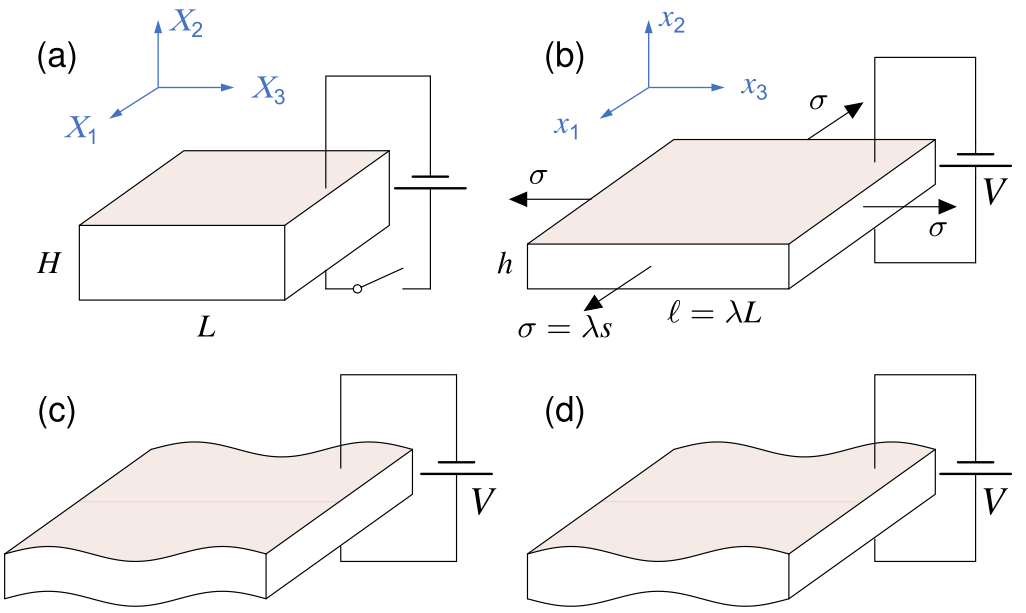

Fig. 3. When put under voltage V and/or stress σ, a rectangular plate made of a soft dielectric and with faces covered by compliant electrodes deforms homogeneously (a) and (b). It can even deform so severely as to lose its stability and buckle into antisymmetric (c) or symmetric (d) modes of wrinkles.

for a plate with no mechanical traction applied on the faces $x_2 = \pm h/2$, where h is the thickness of the deformed plate, we find the following compact expression for the equi-biaxial nominal stress component required to maintain the deformation (Dorfmann and Ogden, 2014a):

$$s = \frac{1}{2}\frac{\partial \omega}{\partial \lambda}, \tag{6}$$

where s is the nominal stress applied along the in-plane directions. For example, for the Gent ideal dielectric we have (Lu et al., 2012)

$$s_G = \mu \frac{\lambda - \lambda^{-5}}{1 - (2\lambda^2 + \lambda^{-4} - 3)/J_m} - \varepsilon \lambda^3 E_0^2, \tag{7}$$

which we can easily invert to find the voltage $V_G = E_0 H$. Here, a non-dimensional measure of V_G is

$$\bar{E}_0 = \frac{V_G}{H\sqrt{\mu/\varepsilon}} = \frac{E_0}{\sqrt{\mu/\varepsilon}} = \sqrt{\frac{\lambda^{-2} - \lambda^{-8}}{1 - (2\lambda^2 + \lambda^{-4} - 3)/J_m} - \lambda^{-3}\bar{s}}, \tag{8}$$

where $\bar{s} = s_G/\mu$ is a non-dimensional measure of stress. We use this formula to plot the non-dimensional loading curves of Fig. 1, as well as the curve for the onset of snap-through, corresponding to $d\bar{E}_0/d\lambda = 0$.

Note that the electric displacement vector $\boldsymbol{D} = (0, D, 0)$, with D being the only non-zero component, is related to the electric field through the formula

$$D = -\lambda_1^{-1}\lambda_3^{-1}\frac{\partial \omega}{\partial E_0}. \tag{9}$$

In this paper we study the possibility of homogeneously deformed plates buckling inhomogeneously as sketched in Fig. 3. Typically, we find that the onset of these buckling modes is governed by a *dispersion equation* relating the critical stretch λ_{cr} to the ratio of the plate thickness H by the wavelength of the wrinkles $\mathcal{L}$. In effect, we find that it can be factorised into the product of a dispersion equation for antisymmetric wrinkles and one for symmetric wrinkles, see Fig. 3(c) and (d).

3. Small-amplitude wrinkles

We now linearize the governing equations and boundary conditions in the neighborhood of the large electro-elastic deformation. We adopt the point of view that the existence of an incremental solution at an equilibrium state implies that the second variation of the energy is not positive definite, and signals the onset of instability, at least in the linearized sense. This connection has been established by several researchers over the years, see for instance the reviews by Sawyers (1996) or Ogden (2000), or the more recent investigation by Chen et al. (2018).

We introduce the following fields: $\boldsymbol{u}$, the small-amplitude mechanical displacement; $\dot{T}_{2i}$, the incremental mechanical traction on the planes x_2 =const.; and $\dot{\boldsymbol{D}}_L$, $\dot{\boldsymbol{E}}_L$, the incremental electric displacement and electric field, respectively. These fields are functions of $\boldsymbol{x}$, the position vector in the current (actuated) configuration (Dorfmann and Ogden, 2014c).

We focus on *two-dimensional wrinkles*, and thus take the fields to be functions of x_1, x_2 only. This leads to (not shown here) $u_3 = \dot{T}_{3i} = \dot{E}_{L3} = \dot{D}_{L3} = 0$. Because the updated, incremental version of the Maxwell equation $\mathrm{Curl}\dot{\boldsymbol{E}}_L = \boldsymbol{0}$ is $\mathrm{curl}\dot{\boldsymbol{E}}_L = \boldsymbol{0}$ (Dorfmann and Ogden, 2010a), we can introduce the electric potential φ by

$$\dot{E}_{L1} = -\partial\varphi/\partial x_1, \qquad \dot{E}_{L2} = -\partial\varphi/\partial x_2. \tag{10}$$

We then seek solutions with sinusoidal shape along x_1 and amplitude variations along x_2, in the form

$$\left\{u_1, u_2, \dot{D}_{L2}, \dot{T}_{21}, \dot{T}_{22}, \varphi\right\} = \Re\left\{\left[k^{-1}U_1, k^{-1}U_2, \mathrm{i}\Delta, \mathrm{i}\Sigma_{21}, \mathrm{i}\Sigma_{22}, k^{-1}\Phi\right]e^{\mathrm{i}kx_1}\right\}, \tag{11}$$

where U_1, U_2, Δ, Σ_{21}, Σ_{22}, Φ are functions of kx_2 only and $k = 2\pi/\mathcal{L}$ is the wavenumber.

Our main result is that the governing equations can be put in the form

$$\boldsymbol{\eta}' = \mathrm{i}\boldsymbol{N}\boldsymbol{\eta}, \tag{12}$$

where

$$\boldsymbol{\eta} = \begin{bmatrix} U_1 & U_2 & \Delta & \Sigma_{21} & \Sigma_{22} & \Phi \end{bmatrix}^T = \begin{bmatrix} \boldsymbol{U} & \boldsymbol{S} \end{bmatrix}^T, \tag{13}$$

is the Stroh vector and the prime denotes differentiation with respect to kx_2. Here $\boldsymbol{U} = \begin{bmatrix} U_1 & U_2 & \Delta \end{bmatrix}^T$, $\boldsymbol{S} = \begin{bmatrix} \Sigma_{21} & \Sigma_{22} & \Phi \end{bmatrix}^T$ are the generalised displacement and traction vectors, respectively, and $\boldsymbol{N}$ is the Stroh matrix. In the appendix we show that $\boldsymbol{N}$ has the following block structure

$$\boldsymbol{N} = \begin{bmatrix} \boldsymbol{N}_1 & \boldsymbol{N}_2 \\ \boldsymbol{N}_3 & \boldsymbol{N}_1 \end{bmatrix}, \tag{14}$$

where the $\boldsymbol{N}_i$ $(i = 1, 2, 3)$ are real symmetric. We find that these 3×3 sub-matrices are

$$\boldsymbol{N}_1 = \begin{bmatrix} 0 & -1 & 0 \\ -1 & 0 & 0 \\ 0 & 0 & 0 \end{bmatrix}, \quad \boldsymbol{N}_2 = \begin{bmatrix} \frac{1}{c} & 0 & \frac{d}{c} \\ 0 & 0 & 0 \\ \frac{d}{c} & 0 & \frac{d^2}{c} - f \end{bmatrix}, \quad \boldsymbol{N}_3 = \begin{bmatrix} \frac{e^2}{g} - 2(b+c) & 0 & -\frac{e}{g} \\ 0 & c-a & 0 \\ -\frac{e}{g} & 0 & \frac{1}{g} \end{bmatrix}, \tag{15}$$

where *a, b, c, d, e, f, g* are electro-elastic moduli. Their general expression in terms of the free energy density Ω is given in the appendix. For equi-biaxial deformations, they read

$$\begin{aligned}
a &= 2\left[\lambda^2(\Omega_1 + \lambda^2\Omega_2) + \lambda^4\left(\Omega_5 + (2\lambda^4 + \lambda^{-2})\Omega_6\right)E_0^2\right],\\
b &= 2\Big\{(\lambda^{-4} - \lambda^2)\left[(\lambda^{-4} - \lambda^2)(\Omega_{11} + 2\lambda^2\Omega_{12} + \lambda^4\Omega_{22}) - 2\lambda^4(\Omega_{15} + 2\lambda^4\Omega_{16} + \lambda^2\Omega_{25} + 2\lambda^6\Omega_{26})E_0^2\right]\\
&\quad + \lambda^8(\Omega_{55} + 4\lambda^4\Omega_{56} + 4\lambda^8\Omega_{66})E_0^4\Big\} + (\lambda^2 + \lambda^{-4})(\Omega_1 + \lambda^2\Omega_2) + \lambda^4\left[\Omega_5 + 2(3\lambda^4 - \lambda^{-2})\Omega_6\right]E_0^2,\\
c &= 2\lambda^{-2}\left[\lambda^{-2}(\Omega_1 + \lambda^2\Omega_2) + \lambda^4\Omega_6E_0^2\right],\\
d &= -2\lambda^2\left[\Omega_5 + (\lambda^4 + \lambda^{-2})\Omega_6\right]E_0,\\
e &= 4\lambda^2\Big[(\lambda^{-4} - \lambda^2)(\lambda^{-4}\Omega_{14} + \Omega_{15} + \lambda^4\Omega_{16} + \lambda^{-2}\Omega_{24} + \lambda^2\Omega_{25} + \lambda^6\Omega_{26})\\
&\quad -\lambda^4(\lambda^{-4}\Omega_{45} + 2\Omega_{46} + \Omega_{55} + 3\lambda^4\Omega_{56} + 2\lambda^8\Omega_{66})E_0^2 - (\Omega_5 + 2\lambda^4\Omega_6)\Big]E_0,\\
f &= 2(\lambda^2\Omega_4 + \Omega_5 + \lambda^{-2}\Omega_6),\\
g &= 4\lambda^4\left[\lambda^{-8}\Omega_{44} + 2\lambda^{-4}\Omega_{45} + 2\Omega_{46} + \Omega_{55} + 2\lambda^4\Omega_{56} + \lambda^8\Omega_{66}\right]E_0^2 + 2(\lambda^{-4}\Omega_4 + \Omega_5 + \lambda^4\Omega_6),
\end{aligned} \tag{16}$$

where $\Omega_i = \partial\Omega/\partial I_i$ and $\Omega_{ij} = \partial^2\Omega/\partial I_i\partial I_j$.

Specializing to the Gent ideal dielectric, we find

$$a = \mu(2\lambda^2\overline{W}' - \lambda^4\overline{E}_0^2), \qquad c = 2\mu\lambda^{-4}\overline{W}', \qquad 2b = 4\mu(\lambda^{-4} - \lambda^2)^2\overline{W}'' + a + c, \tag{17}$$

$$d = \sqrt{\mu\varepsilon}\lambda^2\overline{E}_0, \qquad e = 2\ d, \qquad f = g = -\varepsilon, \tag{18}$$

where

$$\overline{W}' = \frac{1}{2[1 - (2\lambda^2 + \lambda^{-4} - 3)/J_m]}, \qquad \overline{W}'' = \frac{1}{2J_m[1 - (2\lambda^2 + \lambda^{-4} - 3)/J_m]^2}. \tag{19}$$

The Stroh equation must be solved subject to the incremental boundary conditions on the faces of the plate of no mechanical traction and no electrical field, i.e.,

$$\boldsymbol{S}(-kh/2)=\boldsymbol{0},\qquad \boldsymbol{S}(kh/2)=\boldsymbol{0}. \tag{20}$$

Now because the Stroh matrix is constant, the resolution of (12) is straightforward. It reduces to an eigenvalue problem, yielding a complete set of six linearly independent eigensolutions with exponential variations in x_2. Then the boundary conditions give a linear 6×6 homogeneous system of equations for the six unknowns $U_1(\pm h/2)$, $U_2(\pm h/2)$, $\Delta(\pm h/2)$, for which the determinant must be zero: this is the dispersion equation.

Using the usual matrix manipulations of plate acoustics (see Nayfeh, 1995 for instance), the six exponential solutions can be decoupled into two sets of three (hyperbolic) trigonometric solutions, one corresponding to antisymmetric modes, the other to symmetric modes, see sketches in Fig. 3. The dispersion equation itself factorises into two corresponding equations. In the appendix, we give those equations for an arbitrary tri-axial pre-stretch, for materials with free energies of the forms

$$\Omega=W(I_1)-\frac{\varepsilon}{2}I_5,\qquad \Omega=\frac{\mu(1-\beta)}{2}(I_1-3)+\frac{\mu\beta}{2}(I_2-3)-F(I_5), \tag{21}$$

where W and F are arbitrary functions (note that the Gent ideal dielectric belongs to the first type), and $0\le\beta\le 1$ is a constant.

For the Gent ideal dielectric under an equi-biaxial pre-stretch (4), we find the following *explicit dispersion equation for the anti-symmetric wrinkles*:

$$2\overline{W}'\left[p_1(1+p_2^2)^2\tanh\left(\pi p_1\lambda^{-2}H/\mathcal{L}\right)-p_2(1+p_1^2)^2\tanh\left(\pi p_2\lambda^{-2}H/\mathcal{L}\right)\right]=(p_2^2-p_1^2)\lambda^8\overline{E}_0^2\tanh\left(\pi\lambda^{-2}H/\mathcal{L}\right), \tag{22}$$

where

$$p_{1,2}=\frac{\lambda^3+1}{2}\sqrt{1+2(\lambda-\lambda^{-2})^2\frac{\overline{W}''}{\overline{W}'}}\pm\frac{\lambda^3-1}{2}\sqrt{1+2(\lambda+\lambda^{-2})^2\frac{\overline{W}''}{\overline{W}'}}. \tag{23}$$

For symmetric wrinkles, the dispersion equation is the same except that tanh is replaced with coth everywhere.

In the case of the neo-Hookean ideal dielectric (3), we take $J_m\to\infty$ and have $\overline{W}'=1/2$, $\overline{W}''=0$, $p_1=\lambda^3$, $p_2=1$, so that the dispersion equations simplify to

$$\left[\frac{\tanh(\lambda\pi H/\mathcal{L})}{\tanh(\lambda^{-2}\pi H/\mathcal{L})}\right]^{\pm 1}=\frac{(1+\lambda^6)^2}{4\lambda^3}+\frac{\lambda^5(1-\lambda^6)}{4}\overline{E}_0^2, \tag{24}$$

where the $+1$ (-1) exponent corresponds to anti-symmetric (symmetric) wrinkles.

Note that these equations recover the purely elastic buckling criterion when $\overline{E}_0=0$ (Ogden and Roxburgh, 1993).

We now plot the dispersion curves for the Gent ideal dielectric as the plate is loaded homogeneously by an increasing voltage.

When $\overline{E}_0=0$, see Fig. 4(a), we recover the purely mechanical case. The lower/dashed (upper/full) curve corresponds to symmetric (anti-symmetric) buckling. We see that in extension ($\lambda>1$), the plate is always stable, whereas in contraction ($\lambda<1$), it buckles antisymmetrically, with $\lambda_{\rm cr}\simeq 1$ when $H/\mathcal{L}$ is small (thin plate, long wavelength) and $\lambda_{\rm cr}\simeq 0.661$ when $H/\mathcal{L}$ is large (thick plate, short wavelength). Note that here "large" and "thick" simply mean that the plate initial thickness H is of the order of the wavelength $\mathcal{L}$.

When $\overline{E}_0=0.2$, see Fig. 4(b), the landscape is the same, with the curves slightly shifted upwards. The plate only buckles in contraction.

When $\overline{E}_0=0.4$, see Fig. 4(c), we see that, in addition to contractile buckling, the possibility of *wrinkling in extension* has now emerged. The plate buckles anti-symmetrically when λ reaches a critical value $\lambda_{\rm cr}$ between 2.65 (thin-plate limit) and 2.81 (short-wavelength limit), depending on the ratio $H/\mathcal{L}$.

Similarly, when $\overline{E}_0=0.6$, Fig. 4(d) shows that the plate wrinkles anti-symmetrically in extension when λ reaches a critical value $\lambda_{\rm cr}$ between 1.65 (thin-plate limit) and 1.78 (short-wave limit), depending on the ratio $H/\mathcal{L}$.

From this rapid analysis, we conclude that it is unnecessary to study the dispersion equation in detail for the Gent ideal dielectric, and that the thin-plate and short-wave limits suffice to find global, wavelength-independent critical stretches of wrinkling in extension.

4. Thin-plate and short-wave instabilities

In the previous section, we saw that put under a sufficiently large voltage, a dielectric plate wrinkles anti-symmetrically in extension. Depending on the ratio $H/\mathcal{L}$ of thickness to wavelength, the plate wrinkles at a critical stretch located in between a lower bound, corresponding to the limit for thin plates $H/\mathcal{L}\to 0$ and an upper bound, the limit for short wavelengths $H/\mathcal{L}\to\infty$. In this section we present explicit expressions for these two limits.

First, the *thin-plate limit* can be found with the asymptotic behavior of tanh as its argument is small in the dispersion Eq. (22) for the Gent ideal dielectric. However, we can in fact give the thin plate limit in the most general case. Using the

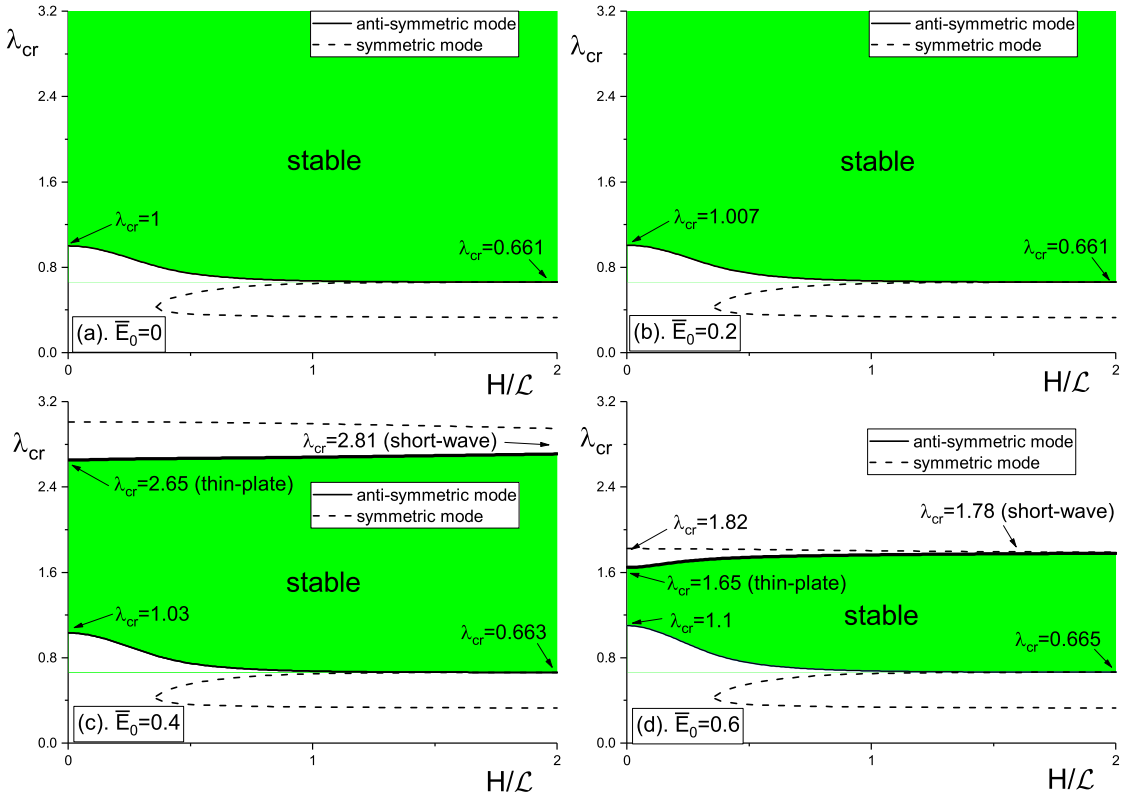

Fig. 4. Dispersion curves for electrically loaded ($\bar{E}_0 = 0.0, 0.2, 0.4, 0.6$) dielectric plates: critical stretch ratio λ_{cr} of compression (lower curves) and of extension (upper curves) against the initial thickness to wavelength ratio $H/\mathcal{L}$. (a) and (b): for low voltages, the plate can wrinkle only in compression. (c) and (d): for higher voltages, the dielectric plate can wrinkle in extension, see the thick upper line, corresponding to anti-symmetric wrinkles. Then, the critical stretch is located between its limit values in the thin-plate ($H/\mathcal{L} \to 0$) and short-wave ($H/\mathcal{L} \to \infty$) limits.

results of Shuvalov (2000), it is easy to show that the buckling condition when $H/\mathcal{L} \to 0$ is simply

$$\det \boldsymbol{N}_3 = 0, \tag{25}$$

where $\boldsymbol{N}_3$ is the Stroh sub-matrix given in Eq. (15). It factorises to give $(a-c)(b+c) = 0$, and the anti-symmetric mode corresponds to $a - c = 0$. Combining Eqs. (5) and (6), we find that $a - c = (\lambda/2)\partial\omega/\partial\lambda$, so that anti-symmetric buckling is equivalent to

$$\frac{\partial \omega}{\partial \lambda} = 0. \tag{26}$$

Comparing with Eq. (6), we see that in general, the loading curve $\bar{E}_0 - \lambda$ with no pre-stress ($\bar{s} = 0$) is in fact the buckling limit for plates of vanishing thickness. This makes sense from a mechanical point of view: a purely elastic membrane with vanishing thickness buckles as soon as it is contracted ($\lambda_{cr} = 1.0$); a dielectric membrane with vanishing thickness can first be stretched by applying a voltage, to $\lambda = \lambda_0$, say, and then it will buckle as soon as it is contracted, so that $\lambda_{cr} = \lambda_0$ now.

Here the equation reads

$$\frac{\lambda^{-2} - \lambda^{-8}}{1 - (2\lambda^2 + \lambda^{-4} - 3)/J_m} = \bar{E}_0^2. \tag{27}$$

Next the *short-wave limit* is found from Eq. (22) by replacing tanh with 1, its value as $H/\mathcal{L} \to \infty$. After some re-arrangement, we find that it reads as

$$2\lambda(\lambda^9 + \lambda^6 + 3\lambda^3 - 1)\overline{W}' + 4(\lambda^6 - 1)^2\overline{W}'' = \lambda^9(1 + \lambda^3)\bar{E}_0^2\sqrt{1 + 2(\lambda - \lambda^{-2})^2\frac{\overline{W}''}{\overline{W}'}}. \tag{28}$$

For example, when $\bar{E}_0 = 0.6$ (and $J_m = 97.2$) we find that the roots to this equation are $\lambda_{cr} = 0.665$ in contraction and $\lambda_{cr} = 1.78$ in extension, as reported on Fig. 4(d). Note that the purely elastic case ($\bar{E}_0 = 0$) is consistent with the surface

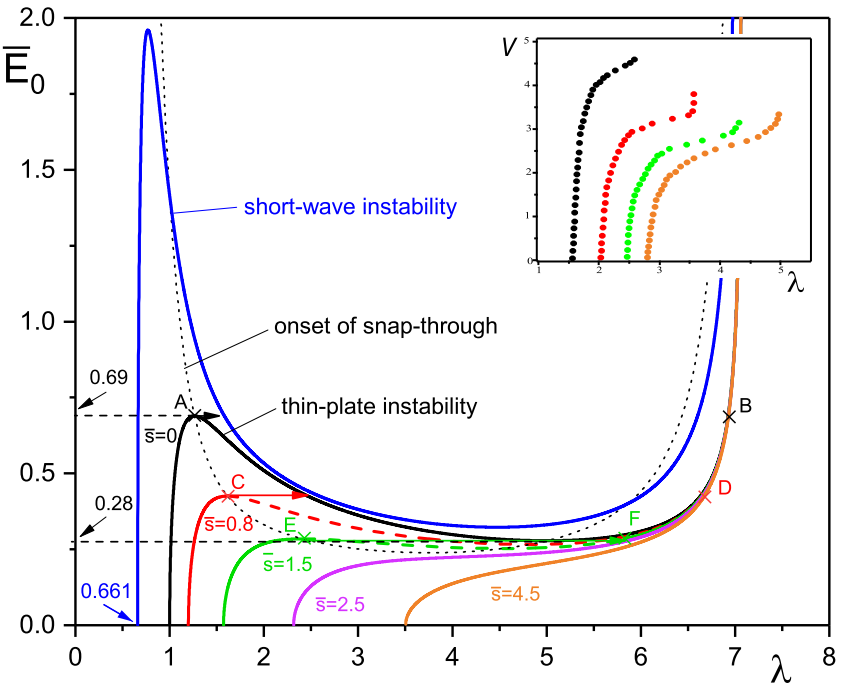

Fig. 5. How the snap-through actuation is counter-acted by plate instabilities. Solid lines are the voltage-stretch curves for homogeneous loading at different levels of pre-stress ($\bar{s} = 0, 0.8, \ldots, 4.5$), when the plate is modeled by the Gent ideal dielectric (here $J_m = 97.2$, Dorfmann and Ogden, 2014b; Gent, 1996). Their intersection with the black dashed line shows where a snap-through should start. However, the non-prestressed plate ($\bar{s} = 0$) will meet the buckling zone found between the thin-plate and the short-wave limit curves on its way from A to B. Similarly for the $\bar{s} = 0.8$ pre-stressed plate. Only the $\bar{s} = 1.5$ pre-stressed plate might be able to experience a snap-through transition from E to F. Inset: experimental voltage (kV) – stretch data digitized from Huang et al. (2012b).

stability criterion of an elastic Gent material (Destrade and Scott, 2004), giving $\lambda_{cr} = 0.661$ here. For the neo-Hookean ideal dielectric of Eq. (3), the equation simplifies to

$$\lambda^9 + \lambda^6 + 3\lambda^3 - 1 = \lambda^8(1 + \lambda^3)\bar{E}_0^2. \tag{29}$$

Note that Dorfmann and Ogden (2014a,c) studied the surface instability of an ideal neo-Hookean dielectric, but it was charge-controlled instead of voltage-controlled as here.

In the purely elastic case ($\bar{E}_0 = 0$), the equation above recovers the critical stretch ratio of surface instability for a half-space under equi-biaxial strain as $\lambda_{cr} = 0.666$, a result which can be traced back to the works of Green and Zerna (1954), Flavin (1963), and Biot (1963a).

Now the two Eqs. (27) and (28) delineate a region in the $\bar{E}_0 - \lambda$ landscape of Fig. 1 where a given plate is going to buckle in contraction when subject to compressive forces and/or wrinkle in extension when subject to a sufficiently large voltage $\bar{E}_0$. The precise value of the corresponding λ_{cr} depends on $H/\mathcal{L}$ but the region between the two curves is narrow enough to draw general conclusions.

In Fig. 5 we plot the loading curves for the same Gent ideal dielectric ($J_m = 97.2$) used to generate the plots of Fig. 1, together with the curves for the thin-plate and short-wave limits. We see that the snap-through scenario is not going to unfold completely for the $\bar{s} = 0$ curve: as soon as $\bar{E}_0$ reaches its maximum (A) and the plate starts expanding with voltage remaining fixed at that value, we enter the wrinkling zone between the thin-plate and the short-wave limits. The same is true for the $\bar{s} = 0.8$ pre-stressed plate, as again, the snap-through from C to D hits the wrinkling zone and cannot be completed. Only the $\bar{s} = 1.5$ pre-stressed plate might be able to achieve a snap-through from E to F without wrinkling.

For plates subject to sufficiently large pre-stress ($\bar{s} = 2.5, 4.5$), the snap-through, thin-plate and short-wave instabilities are avoided, and the plates can deform until they fail by electrical breakdown.

In Fig. 4, we saw that plates buckle in contraction only when $\bar{E}_0$ is small (e.g., $\bar{E}_0 = 0.0, 0.2$, see Fig. 4(a) and (b)), and then in contraction *and* in extension for sufficiently large voltage (e.g., $\bar{E}_0 = 0.4, 0.6$, see Fig. 4(c) and (d)). The critical voltage where the wrinkling in extension is first expressed is determined by

$$\frac{\partial \bar{E}_0}{\partial \lambda} = 0, \quad \text{where} \quad \bar{E}_0 = \sqrt{\frac{\lambda^{-2} - \lambda^{-8}}{1 - (2\lambda^2 + \lambda^{-4} - 3)/J_m}} \tag{30}$$

corresponds to the $\bar{E}_0 - \lambda$ loading curve with no pre-stress ($\bar{s} = 0$).

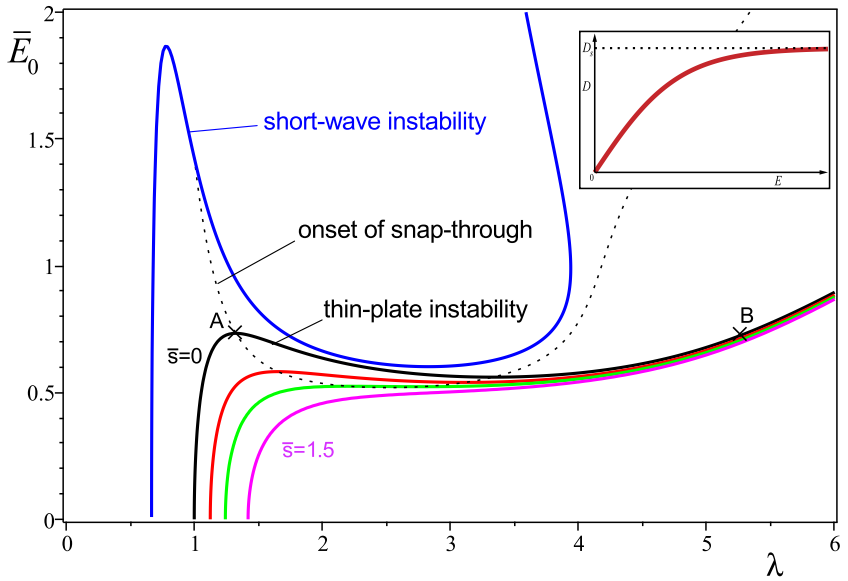

Fig. 6. A dielectric with polarisation saturation: solid lines are the voltage-stretch curves for homogeneous loading at different levels of pre-stress ($\bar{s} = 0, 0.6, 1.0, 1.5$). The non-prestressed plate ($\bar{s} = 0$) will meet the buckling zone found between the thin-plate and the short-wave limit curves on its way from A to B. The pre-stressed plates might be able to avoid buckling, depending on their thickness. Inset: polarisation saturation of the electric displacement with the electric field for the corresponding model (Liu et al., 2012).

In our calculation ($J_m = 97.2$), Eq. (30) has two real roots $\bar{E}_0 = 0.69$ and $\bar{E}_0 = 0.28$. The former corresponds to the voltage at point A (onset of snap-through at the local maximum of the curve) and the latter to the voltage at the local minimum of the curve, see Fig. 5.

Finally, we inserted experimental results in Fig. 5 on actual voltage-stretch curves due to Huang et al. (2012b). They do show that plates can be stretched by voltage a little bit further than the onset of snap-through suggests, by going beyond the maximum of the curve, and that pre-stretch allows for further absolute stretch of the plate by voltage, although the relative gain is affected by the pre-stretch, see Huang et al. (2012b) for a more detailed discussion.

5. Further results

5.1. Plate wrinkling for dielectrics with polarization saturation

Many dielectrics exhibit the phenomenon of *polarization saturation*, in the sense that the electric displacement D increases monotonically with the electric field E but with an asymptotic upper bound D_s, say (Li et al., 2012; 2011b; Liu et al., 2012). This characteristic can be captured by the following form of energy density,

$$\Omega = \frac{\mu(1-\beta)}{2}(I_1 - 3) + \frac{\mu\beta}{2}(I_2 - 3) - \frac{D_s^2}{\varepsilon}\ln\left(\cosh\left(\varepsilon\frac{\sqrt{I_5}}{D_s}\right)\right), \tag{31}$$

where $D_s > 0$ and $0 \le \beta \le 1$ are constants. Then the electric displacement D is related to the electric field E through (see Eq. (9) and Fig. 6),

$$D = D_s \tanh(\varepsilon E/D_s). \tag{32}$$

The nominal stress required to effect an equi-biaxial stretch with a transverse electrical field is found from Eq. (6) as

$$s = \mu(1-\beta)(\lambda - \lambda^{-5}) + \mu\beta(\lambda^3 - \lambda^{-3}) - \lambda D_s E_0 \tanh\left(\lambda^2 \varepsilon E_0/D_s\right). \tag{33}$$

We introduce the following quantities

$$\bar{s} = s/\mu, \qquad \bar{E}_0 = E_0\sqrt{\varepsilon/\mu}, \qquad \bar{D}_s = D_s/\sqrt{\mu\varepsilon}, \tag{34}$$

to obtain the non-dimensional version of this equation as

$$\bar{s} = (1-\beta)(\lambda - \lambda^{-5}) + \beta(\lambda^3 - \lambda^{-3}) - \lambda\bar{D}_s\bar{E}_0 \tanh\left(\lambda^2\bar{E}_0/\bar{D}_s\right). \tag{35}$$

For a given level of pre-stress $\bar{s}$, it gives an implicit relationship between the voltage and the stretch, which we solve to plot the $\bar{E}_0 - \lambda$ curves of Fig. 6. For these plots we took $\beta = 0.2$ and $\bar{D}_s = 4\sqrt{5}$ (corresponding to $k = 1/4$ and $D_s/\sqrt{C_1\varepsilon} = 10$ in

the paper by Liu et al., 2012). We also plot the curve for the onset of snap-through, found by differentiating implicitly Eq. (35) and taking $d\overline{E}_0/d\lambda = 0$.

We note that, as outlined above, the *thin-plate limit* corresponds to this equation in the absence of pre-stress, i.e., when $\bar{s} = 0$. Since the energy density (31) is of the form $(21)_2$, we can make use of the results found using this choice of energy (see appendix, (106)), to obtain the *short-wave limit* as

$$p_3\left[\lambda^{-2}(1-\beta)+\beta\right](\lambda^3+1+3\lambda^{-3}-\lambda^{-6})-(\lambda+\lambda^{-2})\overline{E}_0\overline{D}_s\tanh\left(\lambda^2\overline{E}_0/\overline{D}_s\right)=0, \tag{36}$$

where

$$p_3=\sqrt{\frac{\overline{D}_s}{2\lambda^2\overline{E}_0}\sinh\left(\frac{2\lambda^2\overline{E}_0}{\overline{D}_s}\right)}, \tag{37}$$

is the imaginary part of the third eigenvalue of the corresponding Stroh matrix.

We plotted the thin-plate limit and short-wave limit curves in Fig. 6. We can see that when the material is not under mechanical pre-stress ($\bar{s} = 0$), snap-through does not occur, as the wrinkling zone between the thin-plate and short-wave instabilities is reached before it can be completed. However, we can also see that the plate may avoid buckling when it is pre-stressed, and potentially achieve snap-through, depending on the thickness of the material.

5.2. Correction to the thin-plate buckling equation

Finally, we can exploit the exact dispersion equations to establish approximations to the dispersion equations when the plate is thin. For this exercise, we specialise the analysis to the *Mooney–Rivlin ideal dielectric* model, with free energy density

$$\Omega=\frac{\mu(1-\beta)}{2}(I_1-3)+\frac{\mu\beta}{2}(I_2-3)-\frac{\varepsilon}{2}I_5, \tag{38}$$

where β ($0\le\beta\le1$) is a constant. Note that the neo-Hookean ideal dielectric (3) corresponds to $\beta = 0$.

In this case, the dispersion equation for anti-symmetric wrinkles (the first to appear) reads

$$\frac{\tanh(\lambda\pi H/\mathcal{L})}{\tanh(\lambda^{-2}\pi H/\mathcal{L})}=\frac{(\lambda^2\beta+1-\beta)(1+\lambda^6)^2+\overline{E}_0^2\lambda^8(1-\lambda^6)}{4\lambda^3[1+\beta(\lambda^2-1)]}, \tag{39}$$

which reduces to Eq. (24) for $\beta = 0$. At the zero-th order in $H/\mathcal{L}$, we have the thin-plate equation Eq. (26), here:

$$\overline{E}_0^{-2}=(1-\beta+\beta\lambda^2)(\lambda^{-2}-\lambda^{-8}). \tag{40}$$

This equation has one root (low values of $\overline{E}_0$) or two roots (higher $\overline{E}_0$) for λ, which we call λ_0.

The next order in $H/\mathcal{L}$ is order two. With some manipulations of Eq. (39), we find the following correction,

$$\lambda=\lambda_0-\frac{2}{3}\left[\frac{\lambda_0^3(1-\beta+\beta\lambda_0^2)}{3\beta\lambda_0^2+(1-\beta)(4-\lambda_0^6)}\right](\pi H/\mathcal{L})^2. \tag{41}$$

This expression is valid for both the smallest root of the thin-plate equation (corresponding to buckling in contraction) and the largest root (wrinkling in extension under a large voltage), when it exists. That latter case is a departure from the purely elastic case ($\lambda_0\equiv1$), where there is no loss of stability in extension (Beatty and Pan, 1998). For the neo-Hookean ideal dielectric (3), we take $\beta = 0$ and the expression reduces to

$$\lambda=\lambda_0-\frac{2}{3}\left[\frac{\lambda_0^3}{4-\lambda_0^6}\right](\pi H/\mathcal{L})^2. \tag{42}$$

Finally, $\lambda_0 = 1$ in the purely elastic case, and from Eq. (41) we recover the Euler solution for the buckling of a slender plate under equi-biaxial load: $\lambda = 1-(2/9)(\pi H/\mathcal{L})^2$, see Biot (1963b), Sawyers (1996), or Beatty and Pan (1998) for the connection with the classical formula of the corresponding critical end thrust (see also Yang et al., 2017b).

This type of expansion in $H/\mathcal{L}$ can be performed for any free energy by using the Stroh matrix, see Shuvalov (2000) for details. It allows us to link our stability analysis to that based on the Hessian criterion. That stability criterion is based on minimising the free energy once it has been expanded in terms of the plate thickness up to the first power (Zurlo et al., 2017). It corresponds to the onset of snap-through $d\overline{E}_0/d\lambda = 0$, and of compression-induced failure (De Tommasi et al., 2011). For instance, take the neo-Hookean ideal dielectric (3): in the absence of a pre-stress, the onset of snap-through/Hessian criterion occurs when (Zhao and Suo, 2007)

$$\lambda=2^{1/3}\simeq1.26,\qquad\overline{E}_0=\frac{\sqrt{3}}{2^{4/3}}\simeq0.69. \tag{43}$$

However, Eq. (42) will not work here because the denominator of the correction would be zero. By carefully re-doing the expansion in this special case, we find the first correction to this criterion in terms of the plate thickness to be of order one

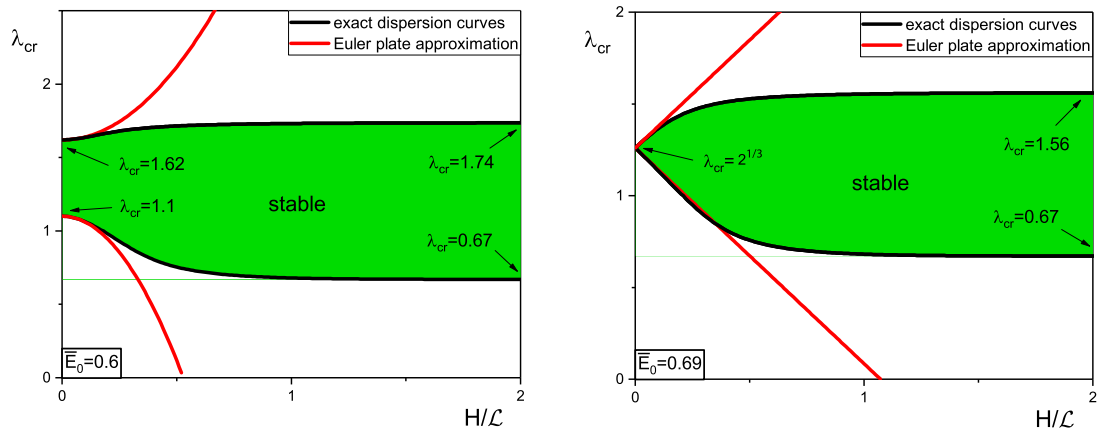

Fig. 7. Critical stretch λ_{cr} versus the initial thickness to wavelength ratio $H/\mathcal{L}$ for the anti-symmetric instability modes of a neo-Hookean ideal dielectric plate (left: $\overline{E}_0 = 0.6$, right: $\overline{E}_0 = \sqrt{3}/2^{4/3} \simeq 0.69$). Black: exact solutions from the analytical dispersion Eq. (24) and red: Euler buckling approximations from Eq. (42) (left) and Eq. $(44)_1$ (right). (For interpretation of the references to color in this figure legend, the reader is referred to the web version of this article.)

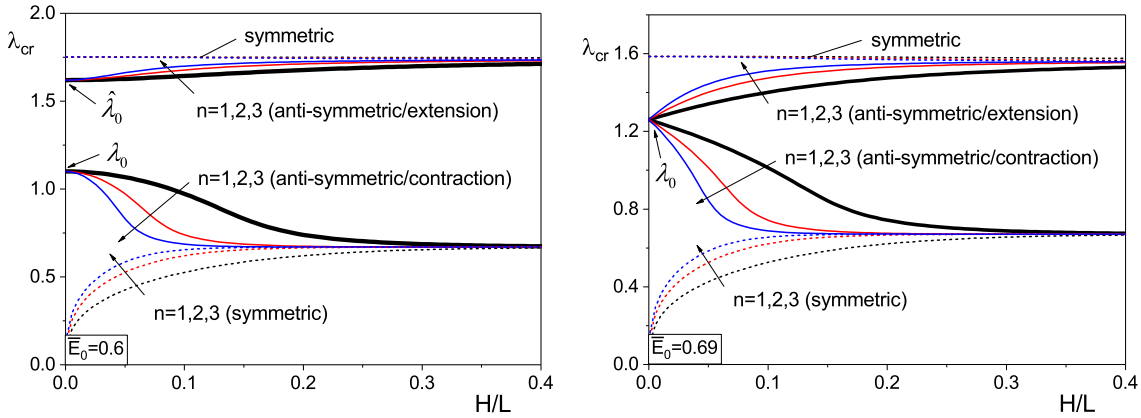

Fig. 8. Dispersion critical curves for an equi-biaxially stretched neo-Hookean ideal dielectric square plate with initial side L and thickness H, in terms of its slenderness H/L, for two levels of voltage: $\overline{E}_0 = 0.6$ (left) and $\overline{E}_0 = \sqrt{3}/2^{4/3} \simeq 0.69$ (right), the value given by the Hessian criterion. The integer n gives the number of half-periods across the plate. We see that the plate can buckle/wrinkle in contraction ($\lambda_{cr} \le \lambda_0$) *and* in extension ($\lambda_{cr} \ge \hat{\lambda}_0$). The plate always buckles/wrinkles anti-symmetrically with one half-period only ($n = 1$, thick black curves). The other modes ($n > 1$ and symmetric modes) are never reached.

for the stretch (and the next term is of order three) and of order two for the voltage (and the next term is of order three). Explicitly,

$$\lambda = 2^{1/3} \pm \frac{2^{1/6}}{3}(\pi H/\mathcal{L}) \simeq 1.26 \pm 1.18(H/\mathcal{L}),$$

$$\overline{E}_0 = \frac{\sqrt{3}}{2^{4/3}} - \frac{2^{1/3}}{3^{3/2}}(\pi H/\mathcal{L})^2 \simeq 0.69 - 2.39(H/\mathcal{L})^2. \tag{44}$$

Fig. 7 shows the dispersion curves obtained by the exact Eq. (24) and the Euler column buckling approximations (42) and $(44)_1$ of a neo-Hookean plate. When $\overline{E}_0 < 0.69$ (left figure), Eq. (41) has two real roots, and the $\lambda_{cr} - H/\mathcal{L}$ curves for the thin plate are approximated quadratically. For the case of the Hessian instability criterion ($\overline{E}_0 = \sqrt{3}/2^{4/3}$), Eq. (41) has a single real root, and the $\lambda_{cr} - H/\mathcal{L}$ curves are approximated linearly for small thicknesses.

The figures confirm the special character of the Hessian criterion to study stability. Prior to reaching the maximum in the voltage-stretch loading curve (for example when $\overline{E}_0 = 0.6$, as in Fig. 7(a)), a thin membrane will buckle when subject to a small amount of contraction (λ_{cr} slightly smaller than $\lambda_0 = 1.1$ in Fig. 7(a)), but can be stretched by a large amount before it wrinkles in extension (the stretch has to reach a value slightly larger than $\lambda_0 = 1.62$). At the Hessian criterion ($\overline{E}_0 = 0.69$), a thin membrane can only be contracted or stretched by a small amount before it buckles or wrinkles (λ_{cr} is close to $\lambda_0 = 2^{1/3}$ for both buckling and wrinkling).

6. Conclusions

6.1. Results of the current paper

Motivated by experimental evidence, we presented a theoretical investigation on the wrinkling modes of instability of a dielectric plate subject to the combined action of electrical voltage in thickness and in-plane equi-biaxial pre-stresses, based on nonlinear electroelasticity and the associated incremental theory. We derived the dispersion equation and decoupled it into explicit antisymmetric and symmetric modes. We recovered classical elastic results of plate buckling when the voltage is absent. For specific energy functions (Gent and neo-Hookean ideal dielectrics, Mooney–Rivlin dielectric with polarization saturation), we obtained the thin-plate and short-wave limits analytically. Our numerical calculations show that plates subject to small-to-moderate voltage require contractile loadings to buckle. For larger applied voltage, the plates can buckle/wrinkle in both contraction and extension, with the critical stretch confined between the thin-plate and short-wave limits. In either case, we found that plates bifurcate anti-symmetrically first and that the symmetric mode is never attained. We determined the threshold value of the voltage where the buckling in extension is first encountered. For thin plates, we extended the Hessian criterion (Zhao and Suo, 2007) to account for thickness terms.

6.2. Lateral boundary conditions: wrinkling, buckling

So far we have not specified the lateral boundary conditions that can be applied on the end faces of the plate, located at $x_1 = 0, \ell_1$ and $x_3 = 0, \ell_3$, say. Instead we wrote our general solution in terms of the wrinkles' wavelength $\mathcal{L}$, because it can handily be specialized to several scenarios.

For instance we may assume that the lateral dimensions of the plate are large enough to ignore the actual boundary conditions on the end faces, and that the only relevant boundary conditions are those applying on the upper and lower faces. This assumption can be used to model loaded plates with a high number of wrinkles, see experimental examples in Fig. 2.

We may also assume that the plate has finite lateral dimensions, say it is a square of initial side length L.

To a given low-to-moderate voltage $\overline{E}_0$ corresponds a single actuation stretch λ_0, say. Here the plate buckles in contraction, when $\lambda = \lambda_{cr} \le \lambda_0$. In practical terms, it means that if we place frictionless walls at $x_1 = 0, \lambda_0 L$, and at $x_3 = 0, \lambda_0 L$, we can push them with equal force against the plate until its side length is $\lambda_{cr} L$, where it buckles. The corresponding wrinkles produce no incremental displacement nor traction in the x_3 direction, so that sliding contact is ensured with the walls at $x_3 = 0, \lambda_0 L$. A short analysis of the incremental fields of the solution (not reproduced here) reveals that both the normal displacement u_1 and the shear traction $\dot{T}_{12}$ are proportional to $\sin(kx_1)$. It follows that the incremental boundary condition of sliding contact with the walls at $x_1 = 0, \lambda_{cr} L$ is fully satisfied when $k\lambda_{cr} L = n\pi$, where n is an integer. We may then replace the $H/\mathcal{L}$ term in the dispersion equations with $n\lambda_{cr}^{-1} H/(2L)$. Hence we used the plate slenderness ratio H/L as a variable to plot Fig. 8, where we solved the dispersion Eq. (24) for a neo-Hookean ideal dielectric for $n = 1, 2, 3$ in turn. We see that the $n = 1$ anti-symmetric mode is always the first one met, in contraction and in extension, so that the plate buckles in a half-period pattern, see sketch 4(a) by Yang et al. (2017b).

For higher voltages, a second, larger activation stretch occurs, at $\lambda = \hat{\lambda}_0$, say. Under those voltages, the plate can buckle in contraction ($\lambda_{cr} \le \lambda_0$) as above, and also in extension ($\lambda_{cr} \ge \hat{\lambda}_0$). At $x_1 = 0, \lambda_{cr} L$, we can apply sliding conditions again, or alternatively, incremental dead-load conditions: $\dot{T}_{11} = \dot{T}_{12} = 0$ (by adjusting the incremental Lagrange multiplier $\dot{p}$). We cannot have $u_1 = 0$ and $u_2 = 0$ simultaneously there, but we can have $u_1 = 0$ and $u_2(0) = u_2(\lambda_{cr} L)$. In that case, the end faces both rise or dip during wrinkling by the same amount, which can be absorbed in the analysis by a superposed translation. Again, we find that the plate wrinkles anti-symmetrically in a half-period pattern.

For the Hessian voltage, we have $\lambda_0 = \hat{\lambda}_0 = 2^{1/3}$ and the plate can buckle in the neighborhood of λ_{cr} both in contraction and in extension with a half-period pattern ($n = 1$). We find from Eq. (44) that the critical stretch is then approximated as

$$\lambda_{cr} = 2^{1/3} \pm \frac{2^{5/6}}{12}(\pi H/L) \simeq 1.26 \pm 0.466(H/L),$$
$$\overline{E}_{0cr} = \frac{\sqrt{3}}{2^{4/3}} - \frac{1}{2^{7/3}3^{3/2}}(\pi H/L)^2 \simeq 0.69 - 0.377(H/L)^2. \tag{45}$$

6.3. Connections with existing results

In the main part of the paper, we presented theoretical and numerical calculations with respect to equi-biaxially deformed plates, but our strategy is readily extended to general tri-axial deformations, see the Appendix. In what follows, we specialise the general results to specific deformations and materials to compare and contrast our results with those of others.

Dorfmann and Ogden (2010b) derived the incremental equations of electro-elasticity and used them to obtain the criterion of surface instability for a class of dielectric models which includes the neo-Hookean model (by taking $\alpha = 0$ in their Eq. (109)). They assumed the dielectric half-space to be immersed in a uniform external electric field and took plane strain conditions. In a later paper (Dorfmann and Ogden, 2014a), they extended the analysis to plates with finite thickness

under equi-biaxial stretch, as here, and considered both the cases of plates immersed in a uniform external field and of electrode-covered plates. In those two investigations, the authors took the Lagrangian electric displacement to be a constant, in contrast to our study, where we take the Lagrangian electric field E_0 to be constant. It follows that we cannot make a direct connection with their results and only give the counterpart explicit dispersion equations below.

Hence, for a *neo-Hookean ideal dielectric plate stretched equi-biaxially*, we found the explicit dispersion equations and surface wrinkling bifurcation criterion as Eqs. (24) and (29), respectively, which we recall below as

$$\left[\frac{\tanh(\pi\lambda H/\mathcal{L})}{\tanh(\pi\lambda^{-2}H/\mathcal{L})}\right]^{\pm 1}=\frac{(1+\lambda^6)^2}{4\lambda^3}+\frac{\lambda^5(1-\lambda^6)}{4}\bar{E}_0^2, \tag{46}$$

(where the $+1/-1$ exponent corresponds to anti-symmetric/symmetric wrinkles), and

$$\lambda^9+\lambda^6+3\lambda^3-1=\lambda^8(1+\lambda^3)\bar{E}_0^2. \tag{47}$$

As shown with the dispersion curves of Fig. 4, these equations are robust and easy to solve numerically, while the determinantal equation of Dorfmann and Ogden (2014a) is probably ill-conditioned, as it presents instability and a merging of symmetric and anti-symmetric modes.

For a *neo-Hookean ideal dielectric plate in plane strain*, we take $\lambda_1=\lambda,\ \lambda_2=1/\lambda,\ \lambda_3=1$ in Appendix Eq. (97), to find the dispersion equations as

$$\left[\frac{\tanh(\pi\lambda H/\mathcal{L})}{\tanh(\pi\lambda^{-1}H/\mathcal{L})}\right]^{\pm 1}=\frac{(1+\lambda^4)^2}{4\lambda^2}+\frac{\lambda^2(1-\lambda^4)}{4}\bar{E}_0^2, \tag{48}$$

and the surface instability equation ($H/\mathcal{L}\to\infty$) as

$$\lambda^6+\lambda^4+3\lambda^2-1=\lambda^4(1+\lambda^2)\bar{E}_0^2. \tag{49}$$

Here the main difference with the equi-biaxial case is that the plane-strain voltage-stretch curve is monotone:

$$\bar{E}_0=\sqrt{1-\lambda^{-4}-\lambda^{-1}\bar{s}}. \tag{50}$$

Because this equation corresponds to the thin-plate limit, it follows that there is now only one possibility of buckling, as to a given voltage corresponds a single actuation stretch λ_0. Here the plate can only buckle in contraction, when $\lambda=\lambda_{\rm cr}\le\lambda_0$.

Díaz-Calleja et al. (2017) took the same set-up as Dorfmann and Ogden (2014a) (in equi-biaxial strain), and also took the electric displacement as constant, so that again, we cannot compare our results to theirs directly. They used an extended Mooney–Rivlin model and an Ogden model in turn, and obtained the dispersion equation as a 6×6 determinant, not decoupled into symmetric and anti-symmetric modes. Their numerical results do not seem to reveal an extensional mode of wrinkling, and seem to present numerical instabilities.

Fu et al. (2018) recently studied the localized necking of ideal neo-Hookean dielectric plates in plane strain. They expanded the bifurcation criterion of Dorfmann and Ogden (2014a) in terms of kH, similar to our analysis in Section 5.2. In an effort to model the initiation of necking in tension, they focused on the symmetric mode of wrinkling. We can also provide such an expression by expanding in a Maclaurin series the bifurcation criterion (48) with the -1 exponent, but there is little value in pursuing this avenue, simply because, as we saw, the symmetric modes are never arrived at, as they are always preceded by anti-symmetric modes.

Finally, Yang et al. (2017b) looked at the buckling of ideal dielectric plates in plane strain. However, when they specialized their results to the neo-Hookean case, they chose for simplicity to not consider the increments in the electrical fields, only in the mechanical fields. As a result they obtained the following dispersion relation, see their Eqs. 69) and ((70),

$$\left[\frac{\tanh(\pi\lambda H/\mathcal{L})}{\tanh(\pi\lambda^{-1}H/\mathcal{L})}\right]^{\pm 1}=\frac{(1+\lambda^4)^2+\lambda^4(1+\lambda^4)\bar{E}_0^2}{4\lambda^2+2\lambda^6\bar{E}_0^2}. \tag{51}$$

The numerical resolution of this equation for the anti-symmetric case shows that it brings little difference compared to the dispersion curve of the exact Eq. (48) for plates subject to small voltages (up to $\bar{E}_0=0.5$, say). However, for larger applied voltage, the difference is quite dramatic, as the equation above under-estimates the critical stretch by at least 15% for thin plates. Also, their equation has roots when $\bar{E}_0>1$, which is not allowed according to (50), see also Yang et al. (2017a). The conclusion is that we must keep all increments (mechanical, electrical, and coupled) to solve the boundary value problem.

6.4. Limitations

Our study is restricted in several ways and can be improved upon.

For example we did not consider viscosity (Hong, 2011; Park and Nguyen, 2013) in any way, although there is strong evidence to support its role in the problem of electro-mechanical instability.

We also discarded the possibility of the wrinkles wavefront being oriented at a different angle instead of being normal to x_1. It could very well be that the first wrinkles to develop are oblique (Carfagna et al., 2017). Further, it could also be the

case that wrinkles with a wavefront normal to x_2 develop. They might even be compatible with our wrinkles and combine to create a two-dimensional pattern (Yin et al., 2018).

Finally, the present incremental theory framework does not seem appropriate to initiate necking (Fu et al., 2018) of a thin plate under large voltage. Our analysis predicts that the $n = 2$ symmetric mode in extension (which is the perfect precursor to necking) can never be attained, as the plate has already reached the bifurcation criterion for the $n = 1$ anti-symmetric mode, where the linearized theory breaks down. Clearly a nonlinear treatment is required to capture necking.

Acknowledgments

This work was supported by a visiting student scholarship for International Collaborative Research from Zhejiang University, a Government of Ireland Postgraduate Scholarship from the Irish Research Council, a Government of Ireland Postdoctoral Fellowship from the Irish Research Council, and the National Natural Science Foundation of China (No. 11621062).

We thank the reviewers and the editor for raising insightful remarks on a previous version of the paper. We are grateful to Yibin Fu (Keele), Ray Ogden (Glasgow) and Giuseppe Zurlo (Galway) for fruitful discussions.

Appendix A

Here, we give the general expressions for the electro-acoustic moduli and the derivation of the Stroh matrix. The appendix is self-contained and some equations from the main text are repeated.

A1. Electro-acoustic moduli

We use the push-forward versions of the incremental constitutive equations when the free energy is of the form $\Omega = \Omega(\boldsymbol{F}, \boldsymbol{E}_L)$ (Dorfmann and Ogden, 2014c):

$$\dot{\boldsymbol{T}} = \mathcal{A}_0\boldsymbol{L} + \boldsymbol{\Gamma}_0\dot{\boldsymbol{E}}_L + p\boldsymbol{L} - \dot{p}\boldsymbol{I}, \qquad \dot{\boldsymbol{D}}_L = -\boldsymbol{\Gamma}_0^T\boldsymbol{L} - \boldsymbol{K}_0\dot{\boldsymbol{E}}_L, \tag{52}$$

where $\dot{\boldsymbol{T}}$ is the push-forward version of the incremental mechanical traction, $\dot{\boldsymbol{E}}_L$ and $\dot{\boldsymbol{D}}_L$ are the push-forward versions of the incremental electric field and electric displacement, respectively, $\boldsymbol{L} = \operatorname{grad}\boldsymbol{u}$ is the gradient of the small-amplitude mechanical displacement $\boldsymbol{u}$, p is the Lagrange multiplier due to the incompressibility condition, with $\dot{p}$ its increment, and $\mathcal{A}_0$, $\boldsymbol{\Gamma}_0$ and $\boldsymbol{K}_0$ are fourth-, third- and second-order tensors, respectively, the so-called *electro-acoustic moduli*.

The electro-acoustic moduli tensors are given in terms of the first and second derivatives of the energy density function Ω with respect to the deformation gradient $\boldsymbol{F}$ and the Lagrangian form of the electric field $\boldsymbol{E}_L = \boldsymbol{F}^T\boldsymbol{E}$, where $\boldsymbol{E}$ is the electric field. Using the invariants given in the main body of the paper, we obtain the following expressions for the components of the moduli tensors,

$$\begin{aligned}
\mathcal{A}_{0jilk} = 4\Big\{&\Omega_{11}b_{ij}b_{kl} + \Omega_{22}(I_1\boldsymbol{b} - \boldsymbol{b}^2)_{ij}(I_1\boldsymbol{b} - \boldsymbol{b}^2)_{kl}\\
&+\Omega_{12}\Big[b_{ij}(I_1\boldsymbol{b} - \boldsymbol{b}^2)_{kl} + b_{kl}(I_1\boldsymbol{b} - \boldsymbol{b}^2)_{ij}\Big] - \Omega_{15}(b_{ij}E_kE_l + b_{kl}E_iE_j)\\
&-\Omega_{16}\Big[b_{ij}(E_k(\boldsymbol{b}^{-1}\boldsymbol{E})_l + (\boldsymbol{b}^{-1}\boldsymbol{E})_kE_l) + b_{kl}(E_i(\boldsymbol{b}^{-1}\boldsymbol{E})_j + (\boldsymbol{b}^{-1}\boldsymbol{E})_iE_j)\Big]\\
&-\Omega_{25}\Big[E_iE_j(I_1\boldsymbol{b} - \boldsymbol{b}^2)_{kl} + E_kE_l(I_1\boldsymbol{b} - \boldsymbol{b}^2)_{ij}\Big] - \Omega_{26}\Big[(I_1\boldsymbol{b} - \boldsymbol{b}^2)_{ij}(E_k(\boldsymbol{b}^{-1}\boldsymbol{E})_l\\
&+(\boldsymbol{b}^{-1}\boldsymbol{E})_kE_l) + (I_1\boldsymbol{b} - \boldsymbol{b}^2)_{kl}(E_i(\boldsymbol{b}^{-1}\boldsymbol{E})_j + (\boldsymbol{b}^{-1}\boldsymbol{E})_iE_j)\Big] + \Omega_{55}E_iE_jE_kE_l\\
&+\Omega_{56}\Big[E_iE_j(E_k(\boldsymbol{b}^{-1}\boldsymbol{E})_l + (\boldsymbol{b}^{-1}\boldsymbol{E})_kE_l) + E_kE_l(E_i(\boldsymbol{b}^{-1}\boldsymbol{E})_j + (\boldsymbol{b}^{-1}\boldsymbol{E})_iE_j)\Big]\\
&+\Omega_{66}(E_i(\boldsymbol{b}^{-1}\boldsymbol{E})_j + (\boldsymbol{b}^{-1}\boldsymbol{E})_iE_j)(E_k(\boldsymbol{b}^{-1}\boldsymbol{E})_l + (\boldsymbol{b}^{-1}\boldsymbol{E})_kE_l)\Big\}\\
&+2\Big\{\Omega_1\delta_{ik}b_{jl} + \Omega_2\Big(2b_{ij}b_{kl} - b_{il}b_{jk} - b_{ik}b_{jl} + \delta_{ik}(I_1\boldsymbol{b} - \boldsymbol{b}^2)_{jl}\Big)\\
&+\Omega_5(\delta_{jl}E_iE_k + \delta_{jk}E_iE_l + \delta_{il}E_jE_k)\\
&+\Omega_6\Big[b_{ik}^{-1}E_jE_l + b_{il}^{-1}E_jE_k + b_{jk}^{-1}E_iE_l + b_{jl}^{-1}E_iE_k + \delta_{jk}(E_i(\boldsymbol{b}^{-1}\boldsymbol{E})_l + (\boldsymbol{b}^{-1}\boldsymbol{E})_iE_l)\\
&+\delta_{il}(E_j(\boldsymbol{b}^{-1}\boldsymbol{E})_k + (\boldsymbol{b}^{-1}\boldsymbol{E})_jE_k) + \delta_{jl}(E_i(\boldsymbol{b}^{-1}\boldsymbol{E})_k + (\boldsymbol{b}^{-1}\boldsymbol{E})_iE_k)\Big]\Big\},
\end{aligned} \tag{53}$$

$$\begin{aligned}
\Gamma_{0jik} = 4\Big\{&b_{ij}\Big[\Omega_{14}(\boldsymbol{b}\boldsymbol{E})_k + \Omega_{15}E_k + \Omega_{16}(\boldsymbol{b}^{-1}\boldsymbol{E})_k\Big]\\
&+(I_1\boldsymbol{b} - \boldsymbol{b}^2)_{ij}\Big[\Omega_{24}(\boldsymbol{b}\boldsymbol{E})_k + \Omega_{25}E_k + \Omega_{26}(\boldsymbol{b}^{-1}\boldsymbol{E})_k\Big]\\
&-E_iE_j\Big[\Omega_{45}(\boldsymbol{b}\boldsymbol{E})_k + \Omega_{55}E_k + \Omega_{56}(\boldsymbol{b}^{-1}\boldsymbol{E})_k\Big]\\
&-\Big(E_i(\boldsymbol{b}^{-1}\boldsymbol{E})_j + (\boldsymbol{b}^{-1}\boldsymbol{E})_iE_j\Big)\Big[\Omega_{46}(\boldsymbol{b}\boldsymbol{E})_k + \Omega_{56}E_k + \Omega_{66}(\boldsymbol{b}^{-1}\boldsymbol{E})_k\Big]\Big\}\\
&-2\Big[\Omega_5(\delta_{jk}E_i + \delta_{ik}E_j) + \Omega_6(\delta_{ik}(\boldsymbol{b}^{-1}\boldsymbol{E})_j + \delta_{jk}(\boldsymbol{b}^{-1}\boldsymbol{E})_i + b_{ik}^{-1}E_j + b_{jk}^{-1}E_i)\Big],
\end{aligned} \tag{54}$$

$$K_{0ij} = 4\Big\{\Omega_{44}(\boldsymbol{bE})_i(\boldsymbol{bE})_j + \Omega_{55}E_iE_j + \Omega_{66}(\boldsymbol{b}^{-1}\boldsymbol{E})_i(\boldsymbol{b}^{-1}\boldsymbol{E})_j + \Omega_{45}\Big[(\boldsymbol{bE})_iE_j + E_i(\boldsymbol{bE})_j\Big] + \Omega_{46}\Big[(\boldsymbol{bE})_i(\boldsymbol{b}^{-1}\boldsymbol{E})_j + (\boldsymbol{b}^{-1}\boldsymbol{E})_i(\boldsymbol{bE})_j\Big] + \Omega_{56}\Big[E_i(\boldsymbol{b}^{-1}\boldsymbol{E})_j + (\boldsymbol{b}^{-1}\boldsymbol{E})_iE_j\Big]\Big\} + 2\Big(\Omega_4 b_{ij} + \Omega_5\delta_{ij} + \Omega_6 b_{ij}^{-1}\Big), \tag{55}$$

where $\boldsymbol{b} = \boldsymbol{F}\boldsymbol{F}^T$ is the left Cauchy–Green deformation tensor, $\Omega_{ij} = \partial^2\Omega/\partial I_i\partial I_j$ and $\Omega_i = \partial\Omega/\partial I_i$, for $i, j = 1, 2, 4, 5, 6$.

These expressions are derived from the derivatives of the invariants with respect to the deformation gradient $\boldsymbol{F}$ and to the Lagrangian electric field $\boldsymbol{E}_L$. The non-zero first derivatives are as follows,

$$\frac{\partial I_1}{\partial F_{i\alpha}} = 2F_{i\alpha}, \qquad \frac{\partial I_2}{\partial F_{i\alpha}} = 2(I_1F_{i\alpha} - c_{\alpha\gamma}F_{i\gamma}),$$

$$\frac{\partial I_5}{\partial F_{i\alpha}} = -2c^{-1}_{\alpha\gamma}E_{L\gamma}F^{-1}_{\delta i}E_{L\delta}, \qquad \frac{\partial I_6}{\partial F_{i\alpha}} = -2\Big(c^{-2}_{\alpha\gamma}E_{L\gamma}F^{-1}_{\delta i}E_{L\delta} + c^{-1}_{\alpha\gamma}E_{L\gamma}c^{-1}_{\delta p}F^{-1}_{pi}E_{L\delta}\Big),$$

$$\frac{\partial I_4}{\partial E_{L\alpha}} = 2E_{L\alpha}, \qquad \frac{\partial I_5}{\partial E_{L\alpha}} = 2c^{-1}_{\alpha\gamma}E_{L\gamma}, \qquad \frac{\partial I_6}{\partial E_{L\alpha}} = 2c^{-2}_{\alpha\gamma}E_{L\gamma}, \tag{56}$$

the non-zero second derivatives with respect to $\boldsymbol{F}$ are

$$\begin{aligned}
\frac{\partial^2 I_1}{\partial F_{i\alpha}\partial F_{k\beta}} &= 2\delta_{ik}\delta_{\alpha\beta},\\
\frac{\partial^2 I_2}{\partial F_{i\alpha}\partial F_{k\beta}} &= 2\Big(2F_{i\alpha}F_{k\beta} - F_{i\beta}F_{k\alpha} + \delta_{ik}(I_1\delta_{\alpha\beta} - c_{\alpha\beta}) - b_{ik}\delta_{\alpha\beta}\Big),\\
\frac{\partial^2 I_5}{\partial F_{i\alpha}\partial F_{k\beta}} &= 2E_{L\gamma}E_{L\delta}\Big(c^{-1}_{\alpha\beta}F^{-1}_{\gamma k}F^{-1}_{\delta i} + c^{-1}_{\beta\gamma}F^{-1}_{\alpha k}F^{-1}_{\delta i} + c^{-1}_{\alpha\gamma}F^{-1}_{\delta k}F^{-1}_{\beta i}\Big),\\
\frac{\partial^2 I_6}{\partial F_{i\alpha}\partial F_{k\beta}} &= 2\Big[c^{-2}_{\alpha\beta}F^{-1}_{\gamma k}F^{-1}_{\delta i} + c^{-2}_{\beta\gamma}F^{-1}_{\alpha k}F^{-1}_{\delta i} + c^{-2}_{\alpha\gamma}F^{-1}_{\delta k}F^{-1}_{\beta i} + c^{-1}_{\alpha\beta}\Big(c^{-1}_{\gamma q}F^{-1}_{qk}F^{-1}_{\delta i}\\
&\quad + c^{-1}_{\delta q}F^{-1}_{qi}F^{-1}_{\gamma k}\Big) + c^{-1}_{\beta\gamma}\Big(c^{-1}_{\alpha q}F^{-1}_{qk}F^{-1}_{\delta i} + c^{-1}_{\delta q}F^{-1}_{qi}F^{-1}_{\alpha k}\Big)\\
&\quad + c^{-1}_{\alpha\gamma}\Big(c^{-1}_{\delta q}F^{-1}_{qk}F^{-1}_{\beta i} + c^{-1}_{\beta q}F^{-1}_{qi}F^{-1}_{\delta k} + c^{-1}_{\beta\delta}b^{-1}_{ik}\Big)\Big]E_{L\gamma}E_{L\delta},
\end{aligned} \tag{57}$$

the non-zero second derivatives with respect to $\boldsymbol{E}_L$ are

$$\frac{\partial^2 I_4}{\partial E_{L\alpha}\partial E_{L\beta}} = 2\delta_{\alpha\beta}, \qquad \frac{\partial^2 I_5}{\partial E_{L\alpha}\partial E_{L\beta}} = 2c^{-1}_{\alpha\beta}, \qquad \frac{\partial^2 I_6}{\partial E_{L\alpha}\partial E_{L\beta}} = 2c^{-2}_{\alpha\beta}, \tag{58}$$

and the mixed second derivatives are

$$\begin{aligned}
\frac{\partial^2 I_5}{\partial F_{i\alpha}\partial E_{L\beta}} &= -2\Big(c^{-1}_{\alpha\beta}F^{-1}_{\gamma i} + c^{-1}_{\alpha\gamma}F^{-1}_{\beta i}\Big)E_{L\gamma},\\
\frac{\partial^2 I_6}{\partial F_{i\alpha}\partial E_{L\beta}} &= -2\Big[c^{-2}_{\alpha\gamma}F^{-1}_{\beta i} + c^{-2}_{\alpha\beta}F^{-1}_{\gamma i} + F^{-1}_{pi}\Big(c^{-1}_{\alpha\gamma}c^{-1}_{\beta p} + c^{-1}_{\alpha\beta}c^{-1}_{\gamma p}\Big)\Big]E_{L\gamma}.
\end{aligned} \tag{59}$$

Note that some of these derivatives were first derived by Rudykh et al. (2014).

A2. Two-dimensional wrinkles in transverse electric field

We look for two-dimensional solutions to the incremental equations so that $\boldsymbol{u} = \boldsymbol{u}(x_1, x_2)$ only. Then $\dot{p}$, $\dot{\boldsymbol{D}}_L$ and $\dot{\boldsymbol{E}}_L$ are also functions of x_1, x_2 only. Although we do not show it here, we find that this leads to $u_3 = 0$, $\dot{D}_{L3} = 0$ and $\dot{E}_{L3} = 0$ for our problem of principal wrinkles in a transverse electrical field. Because curl $\dot{\boldsymbol{E}}_L = \boldsymbol{0}$, we can introduce the electric potential φ and write that

$$\dot{E}_{L1} = -\varphi_{,1}, \qquad \dot{E}_{L2} = -\varphi_{,2}. \tag{60}$$

The push-forward versions of the incremental constitutive equations then have the following non-zero entries,

$$\begin{aligned}
\dot{T}_{11} &= (\mathcal{A}_{01111} + p)u_{1,1} + \mathcal{A}_{01122}u_{2,2} - \Gamma_{0112}\varphi_{,2} - \dot{p},\\
\dot{T}_{12} &= (\mathcal{A}_{01221} + p)u_{1,2} + \mathcal{A}_{01212}u_{2,1} - \Gamma_{0211}\varphi_{,1},\\
\dot{T}_{21} &= (\mathcal{A}_{01221} + p)u_{2,1} + \mathcal{A}_{02121}u_{1,2} - \Gamma_{0211}\varphi_{,1},\\
\dot{T}_{22} &= (\mathcal{A}_{02222} + p)u_{2,2} + \mathcal{A}_{01122}u_{1,1} - \Gamma_{0222}\varphi_{,2} - \dot{p},
\end{aligned} \tag{61}$$

and

$$\dot{D}_{L1} = -\Gamma_{0211}(u_{1,2} + u_{2,1}) + K_{011}\varphi_{,1},$$
$$\dot{D}_{L2} = -\Gamma_{0112}u_{1,1} - \Gamma_{0222}u_{2,2} + K_{022}\varphi_{,2}, \tag{62}$$

because all other components of the electro-elastic moduli are zero. Here $\mathcal{A}_{0jilk}$, Γ_{0jik} and K_{0ij} are given by Eqs. (53), (54) and (55), respectively.

The equilibrium equations in the incremental case, $\mathrm{div}\dot{\boldsymbol{T}} = \boldsymbol{0}$ and $\mathrm{div}\dot{\boldsymbol{D}}_L = 0$, are then as follows,

$$\dot{T}_{11,1} + \dot{T}_{21,2} = 0, \qquad \dot{T}_{12,1} + \dot{T}_{22,2} = 0, \qquad \dot{D}_{L1,1} + \dot{D}_{L2,2} = 0, \tag{63}$$

which together with the incompressibility condition,

$$\mathrm{div}\boldsymbol{u} = u_{1,1} + u_{2,2} = 0, \tag{64}$$

fully describe the incremental motion.

A3. Stroh formulation

We look for solutions that are harmonic in the x_1-direction, i.e., solutions of the form

$$\left\{u_1, u_2, \dot{D}_{L2}, \dot{T}_{21}, \dot{T}_{22}, \varphi\right\} = \Re\{\left[k^{-1}U_1, k^{-1}U_2, \mathrm{i}\Delta, \mathrm{i}\Sigma_{21}, \mathrm{i}\Sigma_{22}, k^{-1}\Phi\right]e^{\mathrm{i}kx_1}\}, \tag{65}$$

where U_1, U_2, Δ, Σ_{21}, Σ_{22} and Φ are functions of kx_2 only, and $k = 2\pi/\mathcal{L}$ is the wavenumber. We can then rewrite the full problem in Stroh form, i.e., as

$$\boldsymbol{\eta}' = \mathrm{i}\boldsymbol{N}\boldsymbol{\eta}, \tag{66}$$

where

$$\boldsymbol{\eta} = \begin{bmatrix} U_1 & U_2 & \Delta & \Sigma_{21} & \Sigma_{22} & \Phi \end{bmatrix}^T = \begin{bmatrix} \boldsymbol{U} & \boldsymbol{S} \end{bmatrix}^T, \tag{67}$$

is the Stroh vector, the prime denotes differentiation with respect to kx_2, and $\boldsymbol{N}$ is the Stroh matrix, which can be partitioned as

$$\boldsymbol{N} = \begin{bmatrix} \boldsymbol{N}_1 & \boldsymbol{N}_2 \\ \boldsymbol{N}_3 & \boldsymbol{N}_1^{\dagger} \end{bmatrix}, \tag{68}$$

where † denotes the Hermitian operator. We derived the Stroh matrix $\boldsymbol{N}$ as follows.

First, substituting u_1 and u_2 into the incompressibility condition, (64), gives

$$U_2' = -\mathrm{i}U_1, \tag{69}$$

the second line of the Stroh equation. We then substitute the expression for $\dot{D}_{L2}$ into Eq. $(62)_2$ and using (69) we get the following expression for Φ',

$$\Phi' = \mathrm{i}\left[\frac{\Gamma_{0112} - \Gamma_{0222}}{K_{022}}U_1 + \frac{1}{K_{022}}\Delta\right], \tag{70}$$

i.e., the last line of the Stroh equation. Similarly, we can then get an expression for U_1' by using $\dot{T}_{21}$ in Eq. $(61)_3$, so that

$$U_1' = \mathrm{i}\left[\frac{-(\mathcal{A}_{01221} + p)}{\mathcal{A}_{02121}}U_2 + \frac{1}{\mathcal{A}_{02121}}\Sigma_{21} + \frac{\Gamma_{0211}}{\mathcal{A}_{02121}}\Phi\right], \tag{71}$$

which is the first line of the Stroh equation.

In order to get the remaining three equations, we use the equilibrium equations Eqs. (63). We first find an expression for $\dot{p}$ by rearranging the expression $(61)_4$ for $\dot{T}_{22}$, and then substitute this into $(61)_1$ and use (70) and $(63)_1$ to find the fourth line of the Stroh equation as follows,

$$\Sigma_{21}' = -\mathrm{i}\left\{\left[\mathcal{A}_{01111} + \mathcal{A}_{02222} - 2\mathcal{A}_{01122} + 2p - \frac{(\Gamma_{0112} - \Gamma_{0222})^2}{K_{022}}\right]U_1 + \Sigma_{22} - \frac{(\Gamma_{0112} - \Gamma_{0222})}{K_{022}}\Delta\right\}. \tag{72}$$

Similarly, we use $(61)_2$, (71) and $(63)_2$ to find the fifth Stroh equation as

$$\Sigma_{22}' = \mathrm{i}\left\{\left[\frac{(\mathcal{A}_{01221} + p)^2}{\mathcal{A}_{02121}} - \mathcal{A}_{01212}\right]U_2 - \frac{(\mathcal{A}_{01221} + p)}{\mathcal{A}_{02121}}\Sigma_{21} - \Gamma_{0211}\left(\frac{\mathcal{A}_{01221} + p}{\mathcal{A}_{02121}} - 1\right)\Phi\right\}. \tag{73}$$

Finally, to get an equation for Δ', we use $(62)_1$, (71) and $(63)_3$ so that,

$$\Delta' = \mathrm{i}\left\{\Gamma_{0211}\left[1 - \frac{(\mathcal{A}_{01221} + p)}{\mathcal{A}_{02121}}\right]U_2 + \frac{\Gamma_{0211}}{\mathcal{A}_{02121}}\Sigma_{21} + \left(\frac{(\Gamma_{0211})^2}{\mathcal{A}_{02121}} - K_{011}\right)\Phi\right\}. \tag{74}$$

We can then write these six equations in the Stroh matrix form. Adopting the following shorthand notation,

$$\begin{aligned} &a = \mathcal{A}_{01212}, \quad c = \mathcal{A}_{02121}, \qquad 2b = \mathcal{A}_{01111} + \mathcal{A}_{02222} - 2\mathcal{A}_{01122} - 2\mathcal{A}_{01221}, \\ &d = \Gamma_{0211}, \quad e = \Gamma_{0222} - \Gamma_{0112}, \quad f = K_{011}, \quad g = K_{022}, \end{aligned} \tag{75}$$

we find the partitions of the Stroh matrix, $\boldsymbol{N}_1$, $\boldsymbol{N}_2$ and $\boldsymbol{N}_3$, as follows,

$$\boldsymbol{N}_1 = \begin{bmatrix} 0 & -1+\tau_{22}/c & 0 \\ -1 & 0 & 0 \\ 0 & d\tau_{22}/c & 0 \end{bmatrix}, \qquad \boldsymbol{N}_2 = \begin{bmatrix} 1/c & 0 & d/c \\ 0 & 0 & 0 \\ d/c & 0 & d^2/c - f \end{bmatrix},$$

$$\boldsymbol{N}_3 = \begin{bmatrix} -2(b+c-\tau_{22}) + e^2/g & 0 & -e/g \\ 0 & -a + (c-\tau_{22})^2/c & 0 \\ -e/g & 0 & 1/g \end{bmatrix}, \tag{76}$$

where we have also made use of the connection $\mathcal{A}_{01221} + p = \mathcal{A}_{02121} - \tau_{22}$ (see Chadwick, 1997 or Shams et al., 2011).

In particular, in this paper, we solve a problem where there is no electric field external to the plate, and so $\tau_{22} = 0$ in the expressions above.

In general, the expressions (75) read as follows,

$$\begin{aligned} a &= 2\big[\lambda_1^2\Omega_1 + \lambda_1^2\lambda_3^2\Omega_2 + \lambda_1^2\lambda_3^2E_0^2\big(\Omega_5 + (\lambda_1^{-2} + 2\lambda_1^2\lambda_3^2)\Omega_6\big)\big], \\ 2b &= 4\Big\{\big(\lambda_1^2 - \lambda_1^{-2}\lambda_3^{-2}\big)\Big[\big(\lambda_1^2 - \lambda_1^{-2}\lambda_3^{-2}\big)\big(\Omega_{11} + 2\lambda_3^2\Omega_{12} + \lambda_3^4\Omega_{22}\big) + 2\lambda_1^2\lambda_3^2E_0^2(\Omega_{15} \\ &\quad +2\lambda_1^2\lambda_3^2\Omega_{16} + \lambda_3^2\Omega_{25} + 2\lambda_1^2\lambda_3^4\Omega_{26})\Big] + \lambda_1^4\lambda_3^4E_0^4\big(\Omega_{55} + 4\lambda_1^2\lambda_3^2\Omega_{56} + 4\lambda_1^4\lambda_3^4\Omega_{66}\big)\Big\} \\ &\quad +2\Big\{\big(\lambda_1^2 + \lambda_1^{-2}\lambda_3^{-2}\big)\big(\Omega_1 + \lambda_3^2\Omega_2\big) + \lambda_1^2\lambda_3^2E_0^2\big[\Omega_5 + 2(3\lambda_1^2\lambda_3^2 - \lambda_1^{-2})\Omega_6\big]\Big\}, \\ c &= 2\big[\lambda_1^{-2}\lambda_3^{-2}\Omega_1 + \lambda_1^{-2}\Omega_2 + \lambda_3^2E_0^2\Omega_6\big], \\ d &= -2\lambda_1\lambda_3\big[\Omega_5 + (\lambda_1^{-2} + \lambda_1^2\lambda_3^2)\Omega_6\big]E_0, \\ e &= 4\lambda_1\lambda_3\big[(\lambda_1^{-2}\lambda_3^{-2} - \lambda_1^2)(\lambda_1^{-2}\lambda_3^{-2}\Omega_{14} + \Omega_{15} + \lambda_1^2\lambda_3^2\Omega_{16} + \lambda_1^{-2}\Omega_{24} + \lambda_3^2\Omega_{25} + \lambda_1^2\lambda_3^4\Omega_{26}) \\ &\quad -\lambda_1^2\lambda_3^2E_0^2(\lambda_1^{-2}\lambda_3^{-2}\Omega_{45} + 2\Omega_{46} + \Omega_{55} + 3\lambda_1^2\lambda_3^2\Omega_{56} + 2\lambda_1^4\lambda_3^4\Omega_{66}) - (\Omega_5 + 2\lambda_1^2\lambda_3^2\Omega_6)\big]E_0, \\ f &= 2(\lambda_1^2\Omega_4 + \Omega_5 + \lambda_1^{-2}\Omega_6), \\ g &= 4\big[\lambda_1^{-4}\lambda_3^{-4}\Omega_{44} + 2\lambda_1^{-2}\lambda_3^{-2}\Omega_{45} + 2\Omega_{46} + \Omega_{55} + 2\lambda_1^2\lambda_3^2\Omega_{56} + \lambda_1^4\lambda_3^4\Omega_{66}\big]\lambda_1^2\lambda_3^2E_0^2 \\ &\quad +2(\lambda_1^{-2}\lambda_3^{-2}\Omega_4 + \Omega_5 + \lambda_1^2\lambda_3^2\Omega_6). \end{aligned} \tag{77}$$

We can *non-dimensionalise* both the Stroh constants and entries of $\boldsymbol{\eta}$ by introducing the following dimensionless moduli,

$$\begin{aligned} &\overline{a} = a/\mu, \quad \overline{b} = b/\mu, \quad \overline{c} = c/\mu, \quad \overline{\tau}_{22} = \tau_{22}/\mu, \\ &\overline{d} = d/\sqrt{\mu\varepsilon}, \quad \overline{e} = e/\sqrt{\mu\varepsilon}, \quad \overline{f} = f/\varepsilon, \quad \overline{g} = g/\varepsilon, \end{aligned} \tag{78}$$

and dimensionless fields,

$$\overline{U}_i = U_i, \qquad \overline{\Sigma}_{2i} = \Sigma_{2i}/\mu, \qquad \overline{\Delta} = \Delta/\sqrt{\mu\varepsilon}, \qquad \overline{\Phi} = \Phi\sqrt{\varepsilon/\mu}, \tag{79}$$

for $i = 1, 2$, where $\overline{X}$ denotes a dimensionless measure of X, and μ and ε are the initial shear modulus and initial permittivity of the dielectric material,

$$\mu = 2(\Omega_1 + \Omega_2)|_{I_1=I_2=3, I_4=I_5=I_6=0}, \qquad \varepsilon = -2(\Omega_4 + \Omega_5 + \Omega_6)|_{I_1=I_2=3, I_4=I_5=I_6=0}. \tag{80}$$

The finite fields can also be non-dimensionalized by introducing

$$\overline{E}_0 = E_0\sqrt{\varepsilon/\mu}, \qquad \overline{D} = D/\sqrt{\mu\varepsilon}, \qquad \overline{I}_\alpha = (\varepsilon/\mu)I_\alpha \quad (\alpha = 4, 5, 6). \tag{81}$$

Once a is replaced by $\mu\overline{a}$, b by $\mu\overline{b}$, etc., the equations of equilibrium can be re-written in their non-dimensional form $\overline{\boldsymbol{\eta}}' = \mathrm{i}\overline{\boldsymbol{N}}\overline{\boldsymbol{\eta}}$. For the rest of the appendix, the overline notation is understood everywhere, and *all quantities are non-dimensional*.

A4. Method of resolution for plates

Since $\boldsymbol{N}$ has constant entries, we look for solutions to (66) in the form,

$$\boldsymbol{\eta}(kx_2) = \boldsymbol{\eta}^0 e^{\mathrm{i}qkx_2}, \tag{82}$$

which results in an eigen-problem for the eigenvalues q and eigenvectors $\boldsymbol{\eta}^0$ of the matrix $\boldsymbol{N}$,

$$(\boldsymbol{N} - q\boldsymbol{I})\boldsymbol{\eta}^0 = \boldsymbol{0}. \tag{83}$$

The characteristic equation associated with this eigen-problem is

$$cgq^6 + [2bg + cf - (d-e)^2]q^4 + [2bf + ag + 2d(d-e)]q^2 + af - d^2 = 0. \tag{84}$$

This equation is bi-cubic in q and does not depend on the Cauchy stress τ_{22} for any choice of energy density function.

After calculating the eigenvalues q_j and eigenvectors $\boldsymbol{\eta}^{(j)}$, $j = 1, 2, \ldots, 6$, for the Stroh matrix $\boldsymbol{N}$, we can construct the solution to (66) for a plate of electroelastic material,

$$\boldsymbol{\eta}(kx_2) = \begin{bmatrix} \boldsymbol{U}(kx_2) \\ \boldsymbol{S}(kx_2) \end{bmatrix} = \sum_{j=1}^{6} c_j \boldsymbol{\eta}^{(j)} e^{\mathrm{i}q_j kx_2}, \tag{85}$$

where c_j for $j = 1, 2, \ldots, 6$ are arbitrary constants to be determined from the boundary conditions. The eigenvalues come in conjugate pairs because the bicubic has real coefficients. We specialise the analysis to free energies for which the q_j are pure imaginary, and so we write them as $q_j = \mathrm{i}p_j$ and $q_{j+3} = -\mathrm{i}p_j$ for $j = 1, 2, 3$, where p_1, p_2, p_3 are real. Then the eigenvectors are also conjugate pairs, $\boldsymbol{\eta}^{(j)} = \overline{\boldsymbol{\eta}^{(j+3)}}$ for $j = 1, 2, 3$.

The incremental equations must be solved subject to the boundary conditions of no incremental mechanical tractions and no incremental electric field on the faces of the plate, i.e., $\boldsymbol{S}(kh/2) = \boldsymbol{S}(-kh/2) = \boldsymbol{0}$. Using this boundary condition and (85), we can write the following matrix equation,

$$\begin{bmatrix} \boldsymbol{S}(kh/2) \\ \boldsymbol{S}(-kh/2) \end{bmatrix} = \begin{bmatrix} F_1E_1^- & F_2E_2^- & F_3E_3^- & F_4E_1^+ & F_5E_2^+ & F_6E_3^+ \\ G_1E_1^- & G_2E_2^- & G_3E_3^- & G_4E_1^+ & G_5E_2^+ & G_6E_3^+ \\ H_1E_1^- & H_2E_2^- & H_3E_3^- & H_4E_1^+ & H_5E_2^+ & H_6E_3^+ \\ F_1E_1^+ & F_2E_2^+ & F_3E_3^+ & F_4E_1^- & F_5E_2^- & F_6E_3^- \\ G_1E_1^+ & G_2E_2^+ & G_3E_3^+ & G_4E_1^- & G_5E_2^- & G_6E_3^- \\ H_1E_1^+ & H_2E_2^+ & H_3E_3^+ & H_4E_1^- & H_5E_2^- & H_6E_3^- \end{bmatrix} \begin{bmatrix} c_1 \\ c_2 \\ c_3 \\ c_4 \\ c_5 \\ c_6 \end{bmatrix} = \boldsymbol{0}, \tag{86}$$

where $F_j = \eta_4^{(j)}$ is the fourth component, $G_j = \eta_5^{(j)}$ is the fifth component, and $H_j = \eta_6^{(j)}$ is the sixth component of the eigenvector $\boldsymbol{\eta}^{(j)}$, and $E_j^{\pm} = e^{\pm p_j kh/2}$, for $j = 1, 2, \ldots, 6$. We also note that since $q_{j+3} = -q_j$, we have $E_{j+3}^{\pm} = E_j^{\mp}$, for $j = 1, 2, 3$.

For our choices of free energy densities, we find that $F_{j+3} = F_j$, $G_{j+3} = -G_j$, $H_{j+3} = H_j$, for $j = 1, 2, 3$. Then some simple linear manipulations (Nayfeh, 1995) of the matrix result in two 3×3 blocks, the antisymmetric and symmetric modes, and its determinant factorises as follows,

$$\begin{vmatrix} F_1C_1 & F_2C_2 & F_3C_3 \\ G_1S_1 & G_2S_2 & G_3S_3 \\ H_1C_1 & H_2C_2 & H_3C_3 \end{vmatrix} \times \begin{vmatrix} F_1S_1 & F_2S_2 & F_3S_3 \\ G_1C_1 & G_2C_2 & G_3C_3 \\ H_1S_1 & H_2S_2 & H_3S_3 \end{vmatrix} = 0, \tag{87}$$

where $C_j = \cosh(p_j kh/2)$ and $S_j = \sinh(p_j kh/2)$. Here the antisymmetric mode is described by the determinant on the left, and the symmetric mode by the one on the right. We then get the following expressions for the dispersion equations in general,

$$hspace * -6ptG_1(F_3H_2 - F_2H_3)\tanh(p_1kh/2) + G_2(F_1H_3 - F_3H_1)\tanh(p_2kh/2) + G_3(F_2H_1 - F_1H_2)\tanh(p_3kh/2) = 0, \tag{88}$$

for the antisymmetric mode and,

$$G_1(F_3H_2 - F_2H_3)\coth(p_1kh/2) + G_2(F_1H_3 - F_3H_1)\coth(p_2kh/2) + G_3(F_2H_1 - F_1H_2)\coth(p_3kh/2) = 0, \tag{89}$$

for the symmetric mode. The quantity kh can be expressed as $kh = 2\pi\lambda_1^{-1}\lambda_3^{-1}H/\mathcal{L}$, where H is the initial thickness of the plate and $\mathcal{L}$ is the wavelength of the wrinkles, two quantities that are easy to measure experimentally.

A5. Examples

Of course, solving the bicubic (84) is quite cumbersome in the general case, but for some special forms of the free energy density, it simplifies quite a lot. Hence, for *generalized neo-Hookean ideal dielectrics*, which are such that

$$\Omega = W(I_1) - \frac{\varepsilon}{2}I_5, \tag{90}$$

where W is an arbitrary function of I_1 only, we find that it factorises as

$$(q^2+1)\left\{q^4 + \left[1 + \lambda_1^4\lambda_3^2 + 2(\lambda_1^3\lambda_3 - \lambda_1^{-1}\lambda_3^{-1})^2\frac{W''}{W'}\right]q^2 + \lambda_1^4\lambda_3^2\right\} = 0. \tag{91}$$

Here we call q_1 and q_2 the two roots of the factorized biquadratic with positive imaginary part.

Now we define all six eigenvalues and the three real numbers p_j by

$$q_1 = -q_4 = \mathrm{i}p_1, \qquad q_2 = -q_5 = \mathrm{i}p_2, \qquad q_3 = -q_6 = \mathrm{i} \quad (p_3 = 1). \tag{92}$$

The real quantities p_1, p_2 are such that

$$p_1^2 p_2^2 = \lambda_1^4\lambda_3^2, \qquad p_1^2 + p_2^2 = 1 + \lambda_1^4\lambda_3^2 + 2(\lambda_1^3\lambda_3 - \lambda_1^{-1}\lambda_3^{-1})^2\frac{W''}{W'}. \tag{93}$$

Solving for real positive p_1, p_2 gives

$$p_{1,2} = \frac{\lambda_1^2\lambda_3 + 1}{2}\sqrt{1 + 2(\lambda_1 - \lambda_1^{-1}\lambda_3^{-1})^2\frac{W''}{W'}} \pm \frac{\lambda_1^2\lambda_3 - 1}{2}\sqrt{1 + 2(\lambda_1 + \lambda_1^{-1}\lambda_3^{-1})^2\frac{W''}{W'}}. \tag{94}$$

The six eigenvectors are

$$\boldsymbol{\eta}^{(1)} = \begin{bmatrix} -\mathrm{i}p_1 \\ 1 \\ -\mathrm{i}p_1\lambda_1\lambda_3 E_0 \\ 2(1+p_1^2)\dfrac{W'}{\lambda_1^2\lambda_3^2} + \lambda_1^2\lambda_3^2 E_0^2 \\ 2\mathrm{i}\dfrac{(\lambda_1^4\lambda_3^2 + p_1^2)}{p_1\lambda_1^2\lambda_3^2}W' \\ -\lambda_1\lambda_3 E_0 \end{bmatrix}, \qquad \boldsymbol{\eta}^{(2)} = \begin{bmatrix} -\mathrm{i}p_2 \\ 1 \\ -\mathrm{i}p_2\lambda_1\lambda_3 E_0 \\ 2(1+p_2^2)\dfrac{W'}{\lambda_1^2\lambda_3^2} + \lambda_1^2\lambda_3^2 E_0^2 \\ 2\mathrm{i}\dfrac{(\lambda_1^4\lambda_3^2 + p_2^2)}{p_2\lambda_1^2\lambda_3^2}W' \\ -\lambda_1\lambda_3 E_0 \end{bmatrix},$$

$$\boldsymbol{\eta}^{(3)} = \begin{bmatrix} 0 \\ 0 \\ \mathrm{i} \\ \lambda_1\lambda_3 E_0 \\ \mathrm{i}\lambda_1\lambda_3 E_0 \\ -1 \end{bmatrix}, \qquad \boldsymbol{\eta}^{(4)} = \overline{\boldsymbol{\eta}^{(1)}}, \qquad \boldsymbol{\eta}^{(5)} = \overline{\boldsymbol{\eta}^{(2)}}, \qquad \boldsymbol{\eta}^{(6)} = \overline{\boldsymbol{\eta}^{(3)}}. \tag{95}$$

From these expressions we deduce the dispersion equation for anti-symmetric buckling (88) in the form

$$\begin{aligned} &2W'\left[p_1(1+p_2^2)^2\tanh\left(\pi\, p_1\lambda_1^{-1}\lambda_3^{-1}H/\mathcal{L}\right) - p_2(1+p_1^2)^2\tanh\left(\pi\, p_2\lambda_1^{-1}\lambda_3^{-1}H/\mathcal{L}\right)\right] \\ &\quad = (p_2^2 - p_1^2)\lambda_1^4\lambda_3^4 E_0^2\tanh\left(\pi\,\lambda_1^{-1}\lambda_3^{-1}H/\mathcal{L}\right). \end{aligned} \tag{96}$$

Here we can take $H/\mathcal{L} \to 0$ and $H/\mathcal{L} \to \infty$ to establish explicit expressions for the thin-plate and the short-wave limits, as in the main text. The equation is valid for any plate made of a generalized neo-Hookean ideal dielectric (90), subject to a bi-axial pre-stretch λ_1, λ_3.

For example, for a neo-Hookean ideal dielectric, we have $W' = 1/2$, $W'' = 0$, $p_1 = 1$, $p_2 = \lambda_1^2\lambda_3$, and the dispersion equations simplify to

$$\left[\frac{\tanh(\pi\lambda_1 H/\mathcal{L})}{\tanh(\pi\lambda_1^{-1}\lambda_3^{-1}H/\mathcal{L})}\right]^{\pm 1} = \frac{(1+\lambda_1^4\lambda_3^2)^2}{4\lambda_1^2\lambda_3} + \frac{(1-\lambda_1^4\lambda_3^2)\lambda_1^2\lambda_3^3}{4}E_0^2. \tag{97}$$

In the short wavelength limit ($H/\mathcal{L} \to \infty$), we find that it can be rearranged as

$$\left(\lambda_1^2\lambda_3\right)^3 + \left(\lambda_1^2\lambda_3\right)^2 + 3\left(\lambda_1^2\lambda_3\right) - 1 = \left(1 + \lambda_1^2\lambda_3\right)\lambda_1^4\lambda_3^4 E_0^2, \tag{98}$$

and we check that the left hand-side is the cubic established by Flavin (1963) for the surface stability of a purely elastic half-space.

Another example of free energy density for which it is possible to make good progress is defined by the following class,

$$\Omega = \frac{\mu(1-\beta)}{2}(I_1 - 3) + \frac{\mu\beta}{2}(I_2 - 3) - F(I_5), \tag{99}$$

where F is an arbitrary function of I_5 only and $0 \le \beta \le 1$. Then we find that the characteristic equation Eq. (84) factorises fully, as

$$(q^2+1)(q^2+\lambda_1^4\lambda_3^2)\left[(2\lambda_1^2\lambda_3^2 E_0^2 F'' + F')q^2 + F'\right] = 0. \tag{100}$$

The six eigenvalues can again be written in terms of three real numbers p_j,

$$q_1 = -q_4 = \mathrm{i}p_1, \qquad q_2 = -q_5 = \mathrm{i}p_2, \qquad q_3 = -q_6 = \mathrm{i}p_3, \tag{101}$$

where

$$p_1 = 1, \qquad p_2 = \lambda_1^2\lambda_3, \qquad p_3 = \sqrt{\frac{F'}{2\lambda_1^2\lambda_3^2 F'' E_0^2 + F'}}. \tag{102}$$

We find that the corresponding eigenvectors are

$$\boldsymbol{\eta}^{(1)} = \begin{bmatrix} \mathrm{i} \\ -1 \\ -2\mathrm{i}\lambda_1\lambda_3 F' E_0 \\ -2\lambda_1^2\lambda_3^2 F'^2 E_0^2 - 2\lambda_1^{-2}\kappa \\ -\mathrm{i}\lambda_3^2(\lambda_1^2 + \lambda_1^{-2}\lambda_3^{-2})\kappa \\ \lambda_1\lambda_3 E_0 \end{bmatrix}, \qquad \boldsymbol{\eta}^{(2)} = \begin{bmatrix} \mathrm{i}\lambda_1 \\ -\lambda_1^{-1}\lambda_3^{-1} \\ 2\mathrm{i}\lambda_1^2\lambda_3 F' E_0 \\ -2\lambda_1\lambda_3 F'^2 E_0^2 - \lambda_1^{-1}\lambda_3(\lambda_1^2 + \lambda_1^{-2}\lambda_3^{-2})\kappa \\ -2\mathrm{i}\lambda_1^{-1}\kappa \\ E_0 \end{bmatrix},$$

$$\boldsymbol{\eta}^{(3)} = \begin{bmatrix} 0 \\ 0 \\ -2\mathrm{i}F' \\ -2p_3\lambda_1\lambda_3 F' E_0 \\ -2\mathrm{i}\lambda_1\lambda_3 F' E_0 \\ p_3 \end{bmatrix}, \qquad \boldsymbol{\eta}^{(4)} = \overline{\boldsymbol{\eta}^{(1)}}, \qquad \boldsymbol{\eta}^{(5)} = \overline{\boldsymbol{\eta}^{(2)}}, \qquad \boldsymbol{\eta}^{(6)} = \overline{\boldsymbol{\eta}^{(3)}}. \tag{103}$$

where

$$\kappa = \lambda_3^{-2} + \beta(1 - \lambda_3^{-2}). \tag{104}$$

We then find that the antisymmetric mode for the *thin-plate limit*, $a - c = 0$, in this case reads

$$2\lambda_1^2 F'^2 E_0^2 + \kappa(\lambda_1^2 - \lambda_1^{-2}\lambda_3^{-2}) = 0, \tag{105}$$

and that the *short-wave limit*, $H/\mathcal{L} \to \infty$, is as follows,

$$p_3\kappa(\lambda_1^3 + \lambda_1\lambda_3^{-1} + 3\lambda_1^{-1}\lambda_3^{-2} - \lambda_1^{-3}\lambda_3^{-3}) - 2\lambda_1^2(\lambda_1 + \lambda_1^{-1}\lambda_3^{-1})F' E_0^2 = 0. \tag{106}$$

References

An, L., Wang, F.F., Cheng, S.B., Lu, T.Q., Wang, T.J., 2015. Experimental investigation of the electromechanical phase transition in a dielectric elastomer tube. Smart Mater. Struct. 24, 035006.

Beatty, M.F., Pan, F.X., 1998. Stability of an internally constrained, hyperelastic slab. Int. J. NonLin. Mech. 33, 867–906.

Bertoldi, K., Gei, M., 2011. Instability in multilayered soft dielectrics. J. Mech. Phys. Solids 59, 18–42.

Biot, M.A., 1963a. Surface instability of rubber in compression. Appl. Sci. Res. 12, 168–182.

Biot, M.A., 1963b. Exact theory of buckling of a thick slab. Appl. Sci. Res. 12, 183–198.

Blok, J., LeGrand, D.G., 1969. Dielectric breakdown of polymer films. J. Appl. Phys. 40 (1), 288–293.

Bortot, E., Shmuel, G., 2018. Prismatic bifurcations of soft dielectric tubes. Int. J. Eng. Sci. 124, 104–114.

Carfagna, M., Destrade, M., Gower, A.L., Grillo, A., 2017. Oblique wrinkles. Phil. Trans. R. Soc. A 375, 20160158.

Chadwick, P., 1997. The application of the Stroh formalism to prestressed elastic media. Math. Mech. Solids 2, 379–403.

Chen, Y.c., Yang, S.Y., Wheeler, L., 2018. Surface instability of elastic half-spaces by using the energy method. Proc. R. Soc. A 474. 20170854

De Tommasi, D., Puglisi, G., Zurlo, G., 2011. Compression-induced failure of electroactive polymeric thin films. Appl. Phys. Lett. 98, 123507.

Destrade, M., 2015. Incremental equations for soft fibrous materials. In: Nonlinear Mechanics of Soft Fibrous Materials. Springer, Vienna, pp. 233–267.

Destrade, M., Scott, N.H., 2004. Surface waves in a deformed isotropic hyperelastic material subject to an isotropic internal constraint. Wave Motion 40, 347–357.

Díaz-Calleja, R., Llovera-Segovia, P., Quijano-López, A., 2017. Complex bifurcation maps in electroelastic elastomeric plates. Int. J. Solids Struct. 113, 70–84.

Dorfmann, L., Ogden, R.W., 2005. Nonlinear electroelasticity.. Acta Mech. 174, 167–183.

Dorfmann, L., Ogden, R.W., 2006. Nonlinear electroelastic deformations. J. Elasticity 174, 99–127.

Dorfmann, L., Ogden, R.W., 2010a. Electroelastic waves in a finitely deformed electroactive material. IMA J. Appl. Math. 75, 603–636.

Dorfmann, L., Ogden, R.W., 2010b. Nonlinear electroelastostatics: incremental equations and stability. Int. J. Eng. Sci. 48, 1–14.

Dorfmann, L., Ogden, R.W., 2014a. Instabilities of an electroelastic plate. Int. J. Eng. Sci. 77, 79–101.

Dorfmann, L., Ogden, R.W., 2014b. Nonlinear response of an electroelastic spherical shell. Int. J. Eng. Sci. 85, 163–174.

Dorfmann, L., Ogden, R.W., 2014c. Nonlinear theory of electroelastic and magnetoelastic interactions. Springer, New York..

Flavin, J., 1963. Surface waves in pre-stressed Mooney material. Q. J. Mech. Appl. Math. 16, 441–449.

Fu, Y.B., Dorfmann, L., Xie, Y.X., 2018. Localized necking of a dielectric membrane. Extreme Mech. Lett. 21, 44–48.

Gei, M., Colonnelli, S., Springhetti, R., 2012. A framework to investigate instabilities of homogeneous and composite dielectric elastomer actuators. In: Proceedings of the Electroactive Polymer Actuators and Devices (EAPAD), 8340, p. 834010.

Gent, A.N., 1996. A new constitutive relation for rubber. Rubber Chem. Technol. 69, 59–61.

Goshkoderia, A., Rudykh, S., 2017. Electromechanical macroscopic instabilities in soft dielectric elastomer composites with periodic microstructures. Eur. J. Mech. A Solid. 65, 243–256.

Green, A.E., Zerna, W., 1954. Theoretical Elasticity. University Press, Oxford.

Hong, W., 2011. Modeling viscoelastic dielectrics. J. Mech. Phys. Solids 59, 637–650.

Huang, J.S., Li, T.F., Chiang Foo, C., Zhu, J., Clarke, D.R., Suo, Z.G., 2012a. Giant, voltage-actuated deformation of a dielectric elastomer under dead load. Appl. Phys. Lett. 100, 041911.

Huang, J.S., Shian, S., Diebold, R.M., Suo, Z.G., Clarke, D.R., 2012b. The thickness and stretch dependence of the electrical breakdown strength of an acrylic dielectric elastomer. Appl. Phys. Lett. 101, 122905.

Jiang, L., Betts, A., Kennedy, D., Jerrams, S., 2015. Investigation into the electromechanical properties of dielectric elastomers subjected to pre-stressing. Mater. Sci. Eng. C 49, 754–760.

Jiang, L., Betts, A., Kennedy, D., Jerrams, S., 2016. Eliminating electromechanical instability in dielectric elastomers by employing pre-stretch. J. Phys. D Appl. Phys. 49, 265401.

Koh, S.J.A., Li, T.F., Zhou, J.X., Zhao, X.H., Hong, W., Zhu, J., Suo, Z.G., 2011. Mechanisms of large actuation strain in dielectric elastomers. J. Polym. Sci. B Pol. Phys. 49, 504–515.

Li, B., Chen, H.L., Qiang, J.H., Hu, S.L., Zhu, Z.C., Wang, Y.Q., 2011a. Effect of mechanical pre-stretch on the stabilization of dielectric elastomer actuation. J. Phys. D Appl. Phys. 44, 155301.

Li, B., Chen, H.L., Qiang, J.H., Zhou, J.X., 2012. A model for conditional polarization of the actuation enhancement of a dielectric elastomer. Soft Matter 8, 311–317.
Li, B., Liu, L.W., Suo, Z.G., 2011b. Extension limit, polarization saturation, and snap-through instability of dielectric elastomers. Int. J. Smart Nano Mat. 2, 59–67.
Li, Z., Wang, Y.X., Foo, C.C., Godaba, H., Zhu, J., Yap, C.H., 2017. The mechanism for large-volume fluid pumping via reversible snap-through of dielectric elastomer. J. Appl. Phys. 122 (8), 084503.
Liu, L.W., Liu, Y.J., Luo, X.J., Li, B., Leng, J.S., 2012. Electromechanical instability and snap-through instability of dielectric elastomers undergoing polarization saturation. Mech. Mater. 55, 60–72.
Liu, X.J., Li, B., Chen, H.L., Jia, S.H., Zhou, J.X., 2016. Voltage-induced wrinkling behavior of dielectric elastomer.. J. Appl. Polym. Sci. 133, 1–8.
Lu, T.Q., Huang, J.S., Jordi, C., Kovacs, G., Huang, R., Clarke, D.R., Suo, Z.G., 2012. Dielectric elastomer actuators under equal-biaxial forces, uniaxial forces, and uniaxial constraint of stiff fibers. Soft Matter 8, 6167–6173.
Nayfeh, A.H., 1995. Wave Propagation in Layered Anisotropic Media: With Application to Composites, Vol. 39. Elsevier.
Ogden, R.W., 2000. Elastic and pseudo-elastic instability and bifurcation. In: Material Instabilities in Elastic and Plastic Solids, Vol. 414. Springer, Vienna, pp. 209–259. CISM International Centre for Mechanical Sciences (Courses and Lectures)
Ogden, R.W., Roxburgh, D.G., 1993. The effect of pre-stress on the vibration and stability of elastic plates. Int. J. Eng. Sci. 31, 1611–1639.
Park, H.S., Nguyen, T.D., 2013. Viscoelastic effects on electromechanical instabilities in dielectric elastomers. Soft Matter 9, 1031–1042.
Pelrine, R., Kornbluh, R., Pei, Q., Joseph, J., 2000. High-speed electrically actuated elastomers with strain greater than 100%. Science 287, 836–839.
Plante, J.S., Dubowsky, S., 2006. Large-scale failure modes of dielectric elastomer actuators. Int. J. Solids Struct. 43, 7727–7751.
Rudykh, S., Bhattacharya, K., 2012. Snap-through actuation of thick-wall electroactive balloons. Int. J. Non-Lin. Mech. 47, 206–209.
Rudykh, S., Bhattacharya, K., de Botton, G., 2014. Multiscale instabilities in soft heterogeneous dielectric elastomers. Proc. Roy. Soc. A 470. 20130618
Rudykh, S., deBotton, G., 2011. Stability of anisotropic electroactive polymers with application to layered media. Z. Angew. Math. Phys. 62, 1131–1142.
Sawyers, K.N., 1996. On the thickness limitation for euler buckling. In: Carroll, M.M., Hayes, M.A. (Eds.), Nonlinear Effects in Fluids and Solids. Springer, Boston, MA, pp. 297–320.
Shams, M., Destrade, M., Ogden, R.W., 2011. Initial stresses in elastic solids: constitutive laws and acoustoelasticity. Wave Motion 48, 552–567.
Shuvalov, A.L., 2000. On the theory of wave propagation in anisotropic plates. Proc. R. Soc. Lond. A 456, 2197–2222.
Su, Y.P., Zhou, W.J., Chen, W.Q., Lü, C.F., 2016. On buckling of a soft incompressible electroactive hollow cylinder. Int. J. Solids Struct 97, 400–416.
Yang, S., Zhao, X., Sharma, P., 2017a. Avoiding the pull-in instability of a dielectric elastomer film and the potential for increased actuation and energy harvesting. Soft Matt. 13, 4552–4558.
Yang, S.Y., Zhao, X.H., Sharma, P., 2017b. Revisiting the instability and bifurcation behavior of soft dielectrics. J. Appl. Mech. 84, 31008.
Yin, S.F., Li, B., Cao, Y.P., Feng, X.Q., 2018. Surface wrinkling of anisotropic films bonded on a compliant substrate. Int. J. Solids Struct. 141, 219–231.
Zhao, X.H., Suo, Z.G., 2007. Method to analyze electromechanical stability of dielectric elastomers. Appl. Phys. Lett. 9, 061921.
Zhao, X.H., Suo, Z.G., 2010. Theory of dielectric elastomers capable of giant deformation of actuation. Phys. Rev. Lett. 104, 178302.
Zurlo, G., Destrade, M., DeTommasi, D., Puglisi, G., 2017. Catastrophic thinning of dielectric elastomers. Phys. Rev. Lett. 118, 078001.